DESIGN OF A NEGATIVE HELIUM ION INJECTION SYSTEM FOR THE 6MV EN TANDEM ACCELERATOR AT iTHEMBA LABORATORY FOR ACCELERATOR BASED SCIENCES.

Kefilwe Veronica Buthelezi

Supervisor: Prof Elias Sideras Haddad

Dissertation submitted in fulfillment of the requirements for the degree of Masters of Science in Applied Radiation Science and Technology

Centre for Applied Radiation Science and Technology

Faculty of Agriculture Science and Technology

North-West University

Republic of South Africa

October 2008

LIBRARY
MAFIKENG CAMPUS
CALL NO.:
2021 -07- 2 7
ACC.NO.:
NORTH-WEST UNIVERSITY

NWU LIBRARY

Declaration

I, the undersigned, Kefilwe Veronica Buthelezi, hereby declare that the work presented in this dissertation except where otherwise indicated, is my own original work and has not been submitted to any university for the purpose of obtaining a degree.

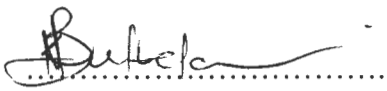

K.V Buthelezi

24-08-09

October 2008

DESIGN OF A NEGATIVE HELIUM ION INJECTION SYSTEM FOR THE 6MV EN TANDEM ACCELERATOR AT iTHEMBA LABORATORY FOR ACCELERATOR BASED SCIENCES.

KEFILWE VERONICA BUTHELEZI

iThemba LABS (Gauteng), Private Bag X 11, Wits 2050, South Africa

October 2008

ABSTRACT

Sufficient production of negative helium ions for acceleration of alpha particles is of great interest in tandem electrostatic accelerator facilities. The Tandem accelerator at iThemba LABS makes use of an 860A Cs-Sputtering negative ion source. This particular procedure assisted by sputtering is totally ineffective for atoms of the inert gasses such as helium (He) due to the electronic stability which also prevents them to form chemical compounds. Therefore an ion source is required to produce negative helium ions for various studies and researches.

A negative-ion source that operates on a different principle other than sputtering has been designed at iThemba LABS. The design is based on a positive Duoplasmatron ion source coupled to a charge-exchange canal. In this, positive helium ions produced in the Duoplasmatron ion source are directed to the charge-exchange canal where through atomic collisions with alkali vapour molecules undergo double-electron capture and become negative. Subsequently, they are injected into the EN 6 MV Tandem accelerator for acceleration.

The physical processes which occur in the exchange canal have also been studied theoretically in order to enhance the understanding of the source behavior. The computer program TRANSPORT is being used for numerical field calculations which guided the design of the source.

AKNOWLEDGEMENTS

I would like to address special thanks to my supervisor Prof Elias Sideras-Haddad for his support, supervision and endless patience in improving my writing.

I am also greatly indebted to iThemba LABS staff for creating a great environment.

I furthermore acknowledge iThemba LABS for providing funds to support this research. I would also like to thank the North West University (NWU) through the Centre of Applied Radiation Science and Technology (CARST) for exposing me to this field.

I need to express my gratitude and deep appreciation to my friends for their kindness, support and encouragement especially Nthabiseng Mashupane whose friendship, hospitality, knowledge and wisdom have supported, enlightened and entertained me over many years of our friendship.

I thank my family: My parents Lesego and Amos Buthelezi for giving me life in the first place, for their unconditional support and encouragement to pursue my interests, even when those interests went beyond their boundaries. I will also like to thank my sister Consolation who has been a friend and a mentor and had confidence in me when i doubted myself. Without her encouragement and constant guidance, I could not have finished this dissertation.

Last but not least the man in my life Matome Mookodi for sharing his experience of the dissertation writing endeavor with me, for listening to my complaints and frustrations, for believing in me and for widening my perspective in life. I LOVE YOU

Of course I would also love to thank God, who gave me all my abilities, for letting all these people enter my life and for molding me into such a wonderful person.

I DEDICATE THIS DISSERTATION TO MY LITTLE ANGEL

REMOFILWE BUTHELEZI

NWU LIBRARY

OUTLINE OF DISSERTATION

The basic structure of the dissertation is as follows:

- The electrostatic accelerators and ion sources in use at iThemba LABS are presented in chapter 1 with the main aim of this study.
- A general theory on negative ion sources as well as the physics models behind the double electron capture is given in chapter 2.
- In chapter 3 a description of the processes for producing negative helium ions are presented.
- Chapter 4 briefly describes the most important beam transport elements and their matrix treatment.
- In chapter 5 the mathematical beam transport formalism for beamlines is introduced. The sigma matrix formalism and first order matrix calculations are emphasized.
- The design considerations of the charge exchange canal of the negative helium ion source are discussed in chapter 6.
- Finally the conclusions drawn from this study are presented in chapter 7.

TABLE OF CONTENTS

ABSTRACT

ACKNOWLEDGEMENTS

OUTLINE

PAGE

CHAPTER 1: MOTIVATION **1-16**

1.1 Introduction 1

1.2 Van de Graaff Accelerators 3

1.3 How Tandem accelerator operates 4

1.4 Source of Negative Ions by Cesium Sputtering (SNICS) 7

1.5 Duoplasmatron Ions Source 10

1.6 Research Aim 13

CHAPTER 2: GENERAL THEORY **17-30**

2.1 Introduction 17

2.2 Negative ion production by charge transfer 17

2.3 Charge exchange processes 18

2.4 Bohr-Lindhard Model 22

2.5 Electron capture to the continuum of neutral projectiles 25

CHAPTER 3: PRODUCTION OF NEGATIVE IONS **31-39**

3.1 Metastable negative ions 31

3.2 Helium energy level 32

3.3 Production on negative helium ions 33

3.3.1 Two step process for production of Negative helium ions 35

CHAPTER 4: BEAM TRANSPORT ELEMENTS 40-45

4.1 Introduction 40

4.2 Drift spaces 40

4.3 Dipole magnets 42

CHAPTER 5 BEAM TRANSPORT FORMALISM 46-66

5.1 Introduction 46

5.2 BEAM optics and TRANSPORT formalism 48

5.3 The BEAM Matrix σ 53

5.4 Description of Sigma BEAM Matrix 55

5.5 The phase ellipse BEAM Matrix used by TRANSPORT 57

5.6 geometric light optics VS magnetic optics 60

5.7 Introduction of momentum dispersion into the matrix formalism 62

CHAPTER 6: CHARGE EXCHANGE CELL DESIGN 67-76

6.1 Introduction 67

6.2 The ion source 70

6.2.1 The Duoplasmatron ion source 70

6.2.2The charge exchange canal 71

6.3 The calculated beam envelope for the designed beamline 75

CHAPTER 7 DISCUSSION AND CONCLUSIONS 77-79

APPENDICES **80-85**

A: THE TRANSPORT INPUT FILE USED FOR THE DESIGN OF BEAMLINE 80

B: THE TRANSPORT OUTPUT FILE 83

REFERENCES **86-90**

CHAPTER 1

MOTIVATION

1.1 INTRODUCTION

Electrostatic accelerators are an important and widespread subgroup within the broad spectrum of modern, large particle acceleration devices. They are specifically designed for applications that require high-quality ion beams in terms of energy stability and emittance at comparatively low energies (a few MeV). Their ability to accelerate different ions over a continuously tunable range of energies renders them a highly versatile tool for investigations in many research fields including, but not limited to, atomic and nuclear spectroscopy, heavy ion reactions, accelerator mass spectrometry (AMS) as well as ion-beam analysis (IBA) and modification of materials **[HILUP]**.

The final energy, quality and intensity of beams delivered by the accelerator depend largely on the charge state, intensity and beam emmitance which can be delivered by a particular ion source. Negative Ion source development, which is the main theme of this study, therefore forms an important part of the activities of a so called Tandem Van de Graaff accelerator laboratory. The technology involved in designing a source depends strongly on the type of particle needed to be generated.

iThemba Laboratory for Accelerator Based Sciences is a multidisciplinary research centre administered by National Research Foundation (NRF).The national facility provides beams of accelerated charged particles used in applied research and also supplies accelerator produced

NWU LIBRARY

radioisotopes for nuclear medicine and nuclear industry. In addition, iThemba LABS operates also the only proton and neutron based therapy for coming patients in Africa. The national facility runs a 200MeV proton four sector cyclotron accelerator and a 6MV single ended Van de Graaff accelerator in Faure-Cape Town. It also operates a 6 MV Tandem electrostatic accelerator in Gauteng which is the only tandem accelerator in operation in the African continent. A schematic diagram of the Tandem laboratory in iThemba Gauteng is shown in figure 1.1.

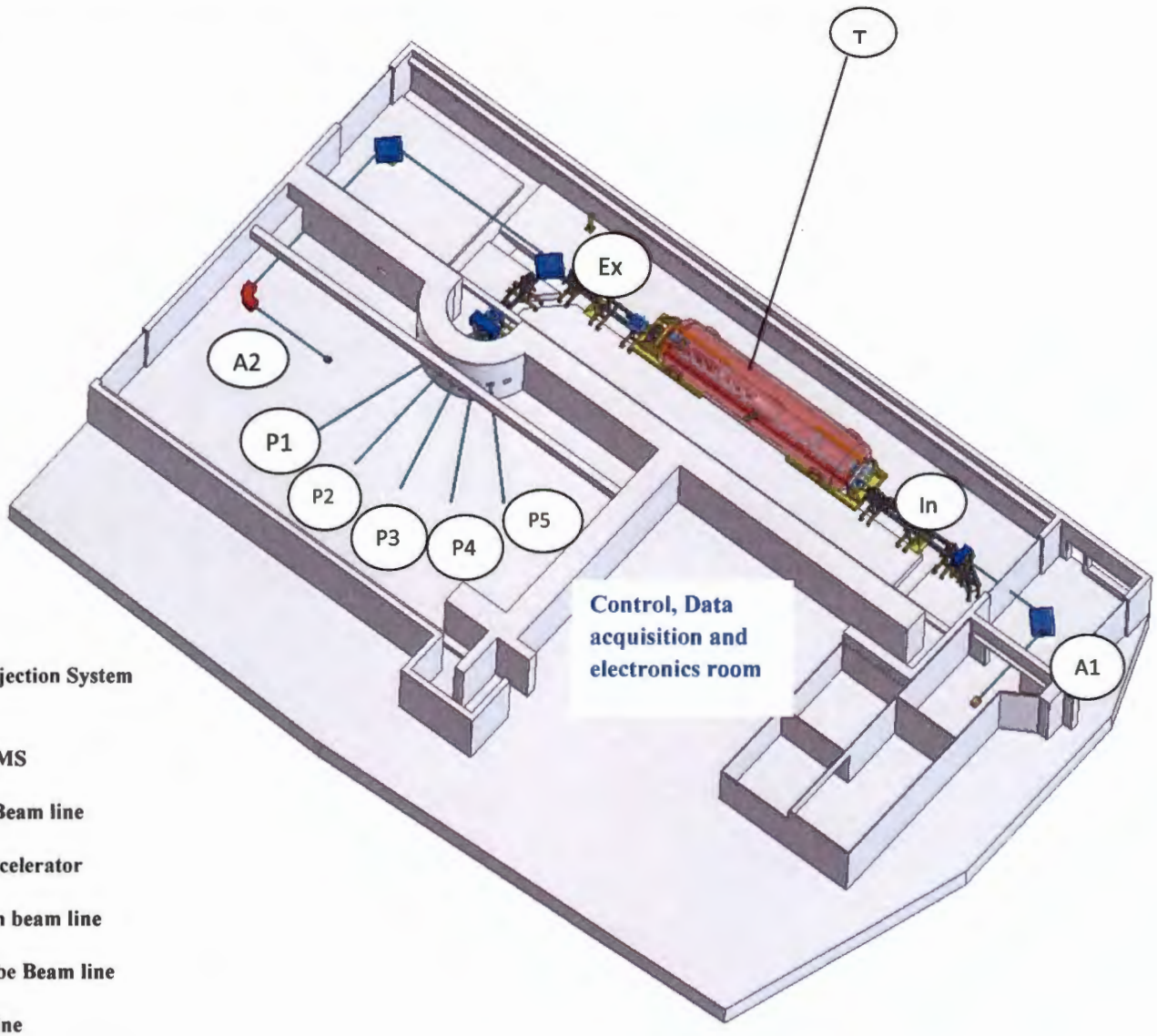

A1: Future Injection System for AMS

A2: Future AMS

In: Injection Beam line

T: Tandem accelerator

Ex: Extraction beam line

P1: Microprobe Beam line

P2: 0 degree line

P3: PIXE

P4: Nuclear Structure line

P5: AMS line

Figure 1.1: Layout of the tandem van de Graaff facility at iThemba LABS Gauteng

1.2 VAN DE GRAAFF ACCELERATORS

A van De Graaff accelerator is an electrostatic machine in which a high potential difference is built up and maintained on a smooth conducting surface by the continuous transfer of positive static charges from a moving belt to the surface. A schematic diagram of a Van de Graaff accelerator is shown in figure 1.2.

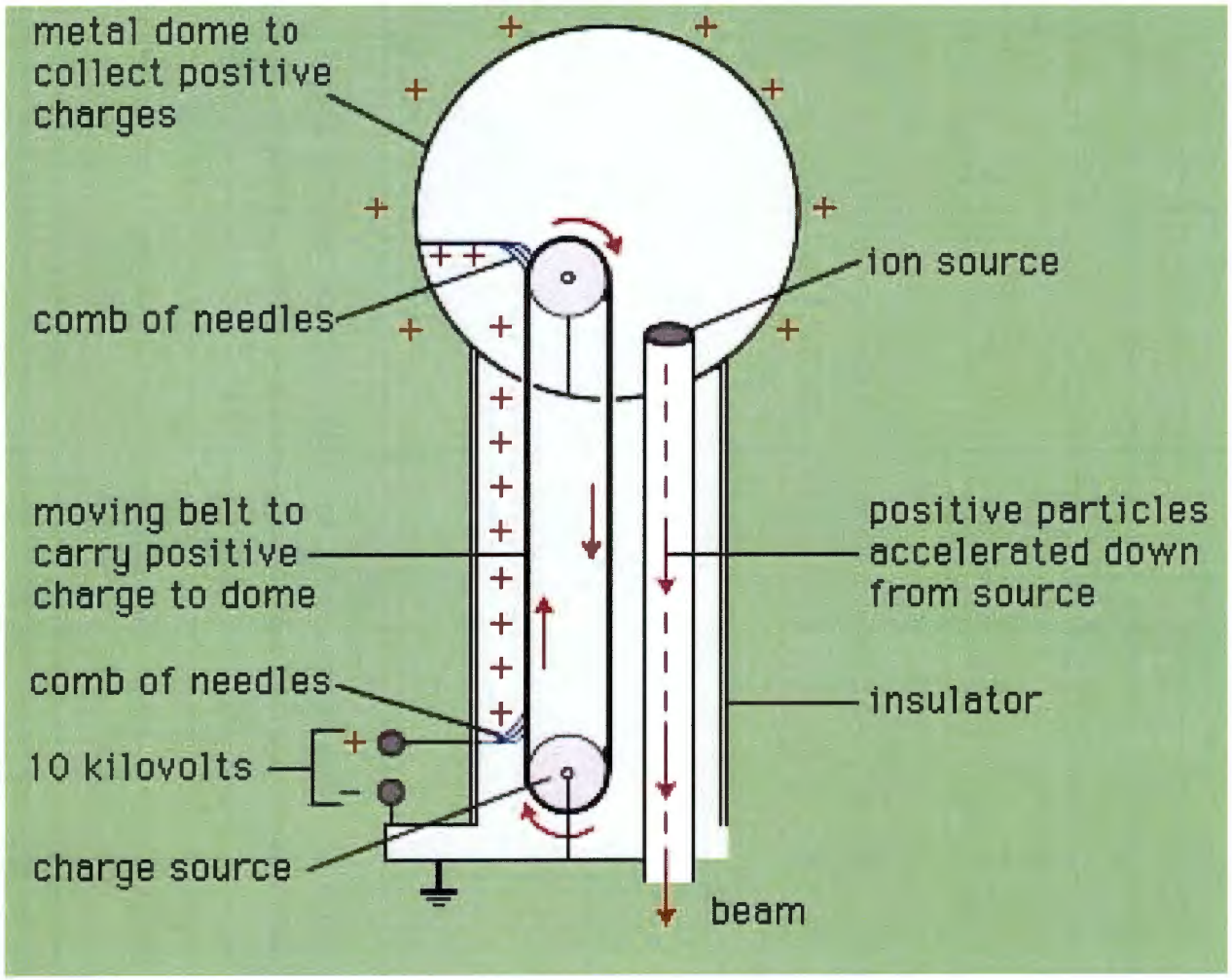

Figure 1.2: A Van de Graaff accelerator **[WWW1]**

In a Van de Graaff accelerator, the high electric potential is coupled to an accelerating tube at the top of which is an ion source that produces the particles to be accelerated. The maximum accelerating potential is limited by breakdown across the accelerating tube and charge leakage from the high voltage electrode. However, with careful design, Van de Graaff accelerators operating at accelerating potentials in excess of 25 MV have been built.

In order to increase the energy of accelerated ions with the same potential Luis Alvarez proposed **[ALV51]** a machine with negative ions accelerated to a positive terminal, stripped and reaccelerated back to ground potential in 1951.

Figure 1.3 shows the general outline of a tandem accelerator, the name Tandem arises from the two acceleration (the one before stripping and the other one after) that the ion beams experience.

1.3 HOW TANDEM ACCELERATOR OPERATES

A tandem is a Van de Graaff electrostatic accelerator with two stages of acceleration; firstly negative ions are extracted from the ion source, the low energy end, (see figure 1.4) mass-analyzed and injected into the accelerator where they are accelerated by the positive potential of the terminal. At the central terminal, they are stripped off one or several electrons through charge exchange processes. The beam is now composed of positive ions with a distribution of different charge states and these ions are now accelerated towards ground potential from the terminal to the high energy end (see figure 1.5). The acceleration of each ion depends on its charge state q so that the final energy E of the ions with charge state q is given by the following equation **[E COTTEREAU]**:

$$E = V_i + (q+1)V_t$$

where: V_i is the initial velocity and V_t is the velocity at the terminal.

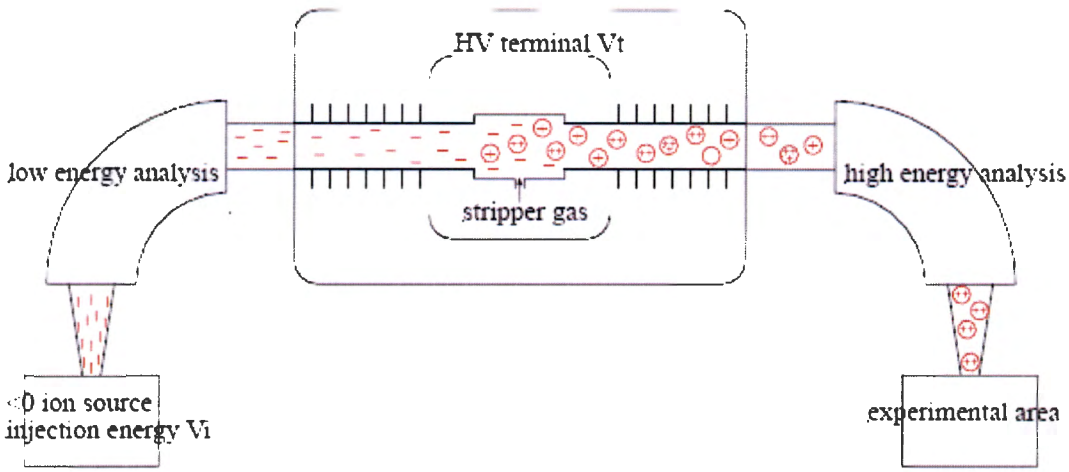

Figure 1.3: Outline of a tandem accelerator. **[E COTTEREAU]**

Another great advantage of the tandem apart from increasing the particle energy is that the ion source is near ground potential and becomes readily accessible. But of course, the double accelerating scheme relies on the availability of adequate negative ion sources.

The stripper can be either a thin carbon foil or a gas depending essentially on the negative ion beam energy and its intensity along with the desired average charge state. Many factors influence the conversion yield such as the nature of the stripper, its density, the energy per nucleon of the incident particles. The thickness of the stripper should be just above the equilibrium thickness that is reached when the cross section out of a charge state is equal to the cross section into it otherwise energy loss effects appear **[E COTTEREAU]**.

Figure 1.4 and 1.5 shows the low energy injection and high energy extraction sections of the Tandem accelerator at iThemba LABS-Gauteng.

Figure 1.4: Injection side of the accelerator (Low energy)

Figure 1.5: Extraction side of the accelerator (High energy)

1.4 SOURCE OF NEGATIVE IONS BY CESIUM SPUTTERING (SNICS)

Naturally occurring negative ions have been proved to be rather elusive particles. The reason for this is that, their electron affinity is almost never greater than 3eV. They are therefore fragile entities and can readily dissociate by collision detachment during interactions with other molecules **[KEN73]**. The existence of the negative ion state has provided physicists with an additional means of producing singly charge negative ion beams containing most of the naturally occurring chemically active elements.

Negative ion beams have been used for many years in high-energy, accelerator-based atomic nuclear and applied research, as well as low-energy fundamental atomic physics and controlled thermonuclear research programs. Such negative ion applications have provided an impetus for the development of sources capable of producing negative ion beams containing almost every element in the periodic chart [**ALT93**]. Sources generally are characterized by the particular mechanism employed for production of negative ions, e.g., charge exchange, volume production in plasmas, sputtering etc. In some cases, more than one mechanism may be involved in the formation process. The sources vary in operational and mechanical complexity, depending on the method required to produce the desired ion species and beam intensity for the particular application **[HEL05]**

The probability for ion formation also depends on the atomic structure properties of the particular atom or molecule [**ALT93**]. The mechanism utilized for positive ion formation may be general in terms of species capabilities. While electron impact ionization offers a specific independent method for positive ion formation, no such universal method exists for producing

negative ion. As a result, specific methods must be employed for the formation of negative ions that depends on the element of interest such as helium.

Cs-sputtering sources are the most commonly used ion beam source for Tandem accelerators. In these sources, a reservoir of cesium is heated to approximately 120 °C, so that cesium vapor is formed. This vapor rises from the reservoir in vacuum to an enclosed region between the cathode, which is cooled, and the ionizer, which is heated. Some of the cesium condenses onto the cool surface of the cathode, while some of the cesium comes in contact with the surface of the ionizer, gets ionized by thermionic emission and is immediately "boiled away". The positively charged cesium ions leaving the ionizer are accelerated toward and focused onto the cathode, sputtering material from the cathode at impact. Some of the sputtered material gains an electron in passing through the cesium coating on the surface of the cathode, and forms the negatively charged beam. The entire source is operated at approximately 30-50 kV below ground, this negative beam is accelerated out of the source and is available for injection into the Tandem accelerator with energies between 30-50keV.

A wide variety of ion beams can be produced with this source, depending upon the nature of the cathode used. The cathode is a cylindrical section of copper, which has a small cavity drilled into the cylinder on axis. Typically, a powder containing the isotope for which beam is desired is tamped into the cavity, to be sputtered out of the cavity by the cesium beam. Whenever possible, the cathodes are prepared in advance, but preparing a new cathode from fresh powder is a relatively simple task. Cathode lifetime varies with isotope, with some lasting for a week or more of continuous duty. However, cathodes can be changed in a relatively short time, so that many cathodes can be used to complete an experiment, if required. The source could be used to

produce beams other than helium, using other gases in the filament region. Figure1.6 shows a schematic diagram of a SNICS source.

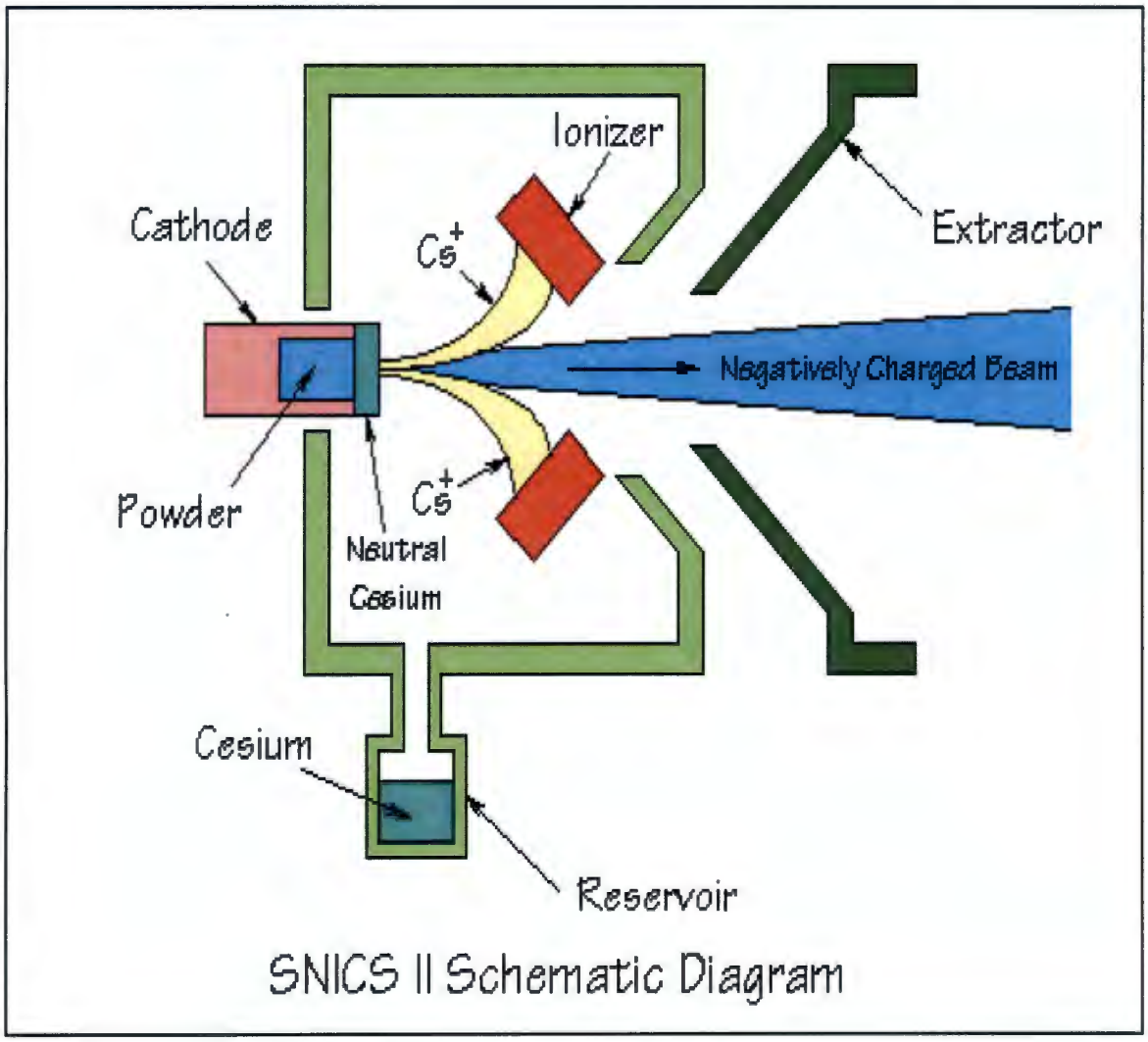

Figure 1.6: Schematic diagram of the Source of Negative Ions by Cesium sputtering **[WWW2]**

The sputter sources have several advantages, that is:

- negative ions can be formed from almost all element,
- ion species can be changed quickly ,

NWU LIBRARY

- intensities are fairly high,
- the ionization efficiency is good,
- the emittance and the energy spread are low **[E COTTEREAU, MID83].**

The negative ion yields from sputter sources are adequate for a wide variety of nuclear experiments and ion beam analysis techniques but some exceptions do occur particularly with elements having small electron affinities **[MID83]**. Unfortunately, this procedure is not effective for ions of inert gases such as helium because they are not reactive under normal circumstances. The tendency for non-reactivity is due to the valence of the outermost electron shell being complete.

1.5 DUOPLASMATRON ION SOURCE

The duoplasmatron ion source was first designed and built by Von Ardenne and is utilized in scientific research and in a variety of industrial applications. The source can be adapted to suit the requirements of a variety of users in different fields **[MOK02]**. It can also be used for production of positive helium () ions. Both cold and hot cathode sources are in use. As the name indicates the discharge is formed in two-stages: the first between the filament, which acts as cathode, and the intermediate electrode at a relatively high pressure and low voltage, and secondly between the intermediate electrode and the anode. Electrons, generated by thermionic emission at the cathode, are accelerated towards the anode and along the way collide with gas molecules, thereby causing dissociation of the gas molecules, ionization of the atoms and formation of plasma in the region between these electrodes.

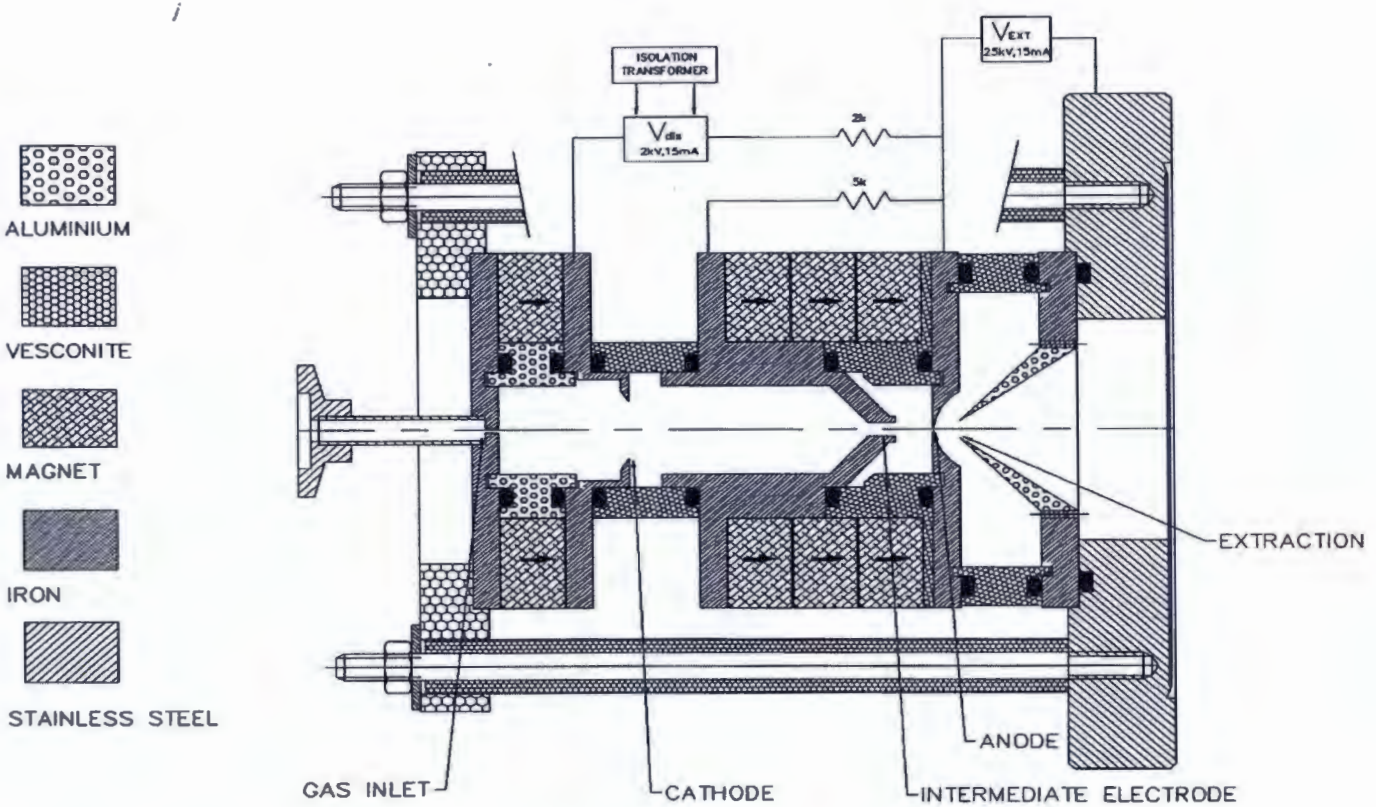

Figure 1.7: A schematic diagram of a Duoplasmatron ion source showing all major components. **[MOK02]**

The electrical field, due to the voltage different between the cathode and the intermediate electrode, shift the plasma towards the anode. The strong magnetic field compresses the plasma and guides it to flow through the orifice in the intermediate electrode into the second stage where plasma is formed between the intermediate electrode and the anode. A combination of the magnetic and the electric fields is employed to constrict the motion of electrons and ions through the anode aperture and thus increasing the interaction cross-section resulting in increased ionization. In the second stage the discharge pressure is much lower and the voltage much higher than in the first stage. The anode has a small aperture through which the plasma flows into the extraction region. The geometry of these electrodes can be varied to optimize the output of the ion source and its general beam optics characteristics. Expansion cups can also be fixed to the anode to allow the plasma to expand before extraction and this can improved the extracted beam current. Typical H+ beam production is of the order of ~100μA.

Ions leave the Duoplasmatron ion source from any point in the exit aperture, with a spread in their initial velocities, both in terms of magnitude and direction, which is caused by the high temperatures inside the ion source and the consequent collisions between the particles. The velocity spread in the beam may be considerably larger than what would be expected from the temperature alone, since temperature fluctuations in the plasma, plasma instabilities and non-linear forces due to external fields and space charge lead to an increase in the velocity spread. A beam from an ion source has therefore, in addition to its height and width, a momentum spread and angular divergence in both the horizontal and vertical directions. Different permutations of these parameters define the quality of beam extracted from the ion source **[MOK02].**

1.6 RESEARCH AIM

Acceleration of α-particles for use in Ion Beam Analysis (IBA) techniques such as Rutherford Back Scattering (RBS), channeling and Nuclear Reaction Analysis (NRA) is of great interest in tandem electrostatic accelerator facilities. The Tandem accelerator at iThemba LABS makes use of an 860A Cs-Sputtering negative ion source. This particular procedure assisted by sputtering is totally ineffective for atoms of the inert gasses such as helium (He) (α-particles) due to their electronic stability which also prevents them to form chemical compounds. Therefore ion sources that operates in different principle other than sputtering need to be designed. The development of an ion source for a particular application should be made with due consideration of factors such as species and intensity capability, beam quality (emittance and brightness), ionization efficiency, material utilization efficiency, reliability, ease of operation, and maintenance, duty cycle and source lifetime. These factors are not of equal importance and the ion source development process should be based on the most desirable combination of characteristics for the particular application **[ALT93]**

A new source design should cater for good beam qualities in terms of the following characteristics:

- beam intensity-luminosity
- stability,
- emmitance,
- long source life time,
- high ionization efficiency
- electron affinity

The processes involved in the attachment of the electron to neutral atoms or molecules are exothermic in contrast to the endothermic processes required for positive ion formation [**ALT93**]. The parameter that characterizes the negative state is the binding energy of the additional attached electron, or the electron affinity E_a **[HEL05].** The binding energy or electron affinity E_a of negative ions is a measure of the stability and ease of negative ion formation. The electron affinity E_a is defined as the difference of the energy between the ground states of the neutral atom (E_0) and of the negative ion (E_-) as sown in the following equation.

$$E_a = E_0 - E_-$$

The electron affinity must be positive for negative ion formation. Table 1 displays experimentally determined electron affinities many of which were taken from the compilation of H Hotop et al **[HOT75].**

The probability therefore of negative ion formation depends significantly on the value of E_a as well as on the method used in the formation process [**ALT93].**

The main objectives of this study are therefore a) to design an ion source that can produce negative helium ions (He^-) ions, which eventually become accelerated α-particle beams from the tandem accelerator since it is impossible to produce negative helium ions using a Cesium (Cs) sputtering negative ion source, due to the high electron stability which also prevent them to form chemical compound and b)to understand the physics of double electron capture by positive ions in terms of cross sections, colliding partners and incident energies and c) to match it in terms of beam optics to the existing Tandem accelerator laboratory.

GROUP 1A							VIII A
1 H 13.595 0.7542 ← Ionization Potential ← Electron Affinity	II A	III A	IV A	V A	VI A	VII A	2 He 24.58 0.078
3 Li 5.39 0.618	4 Be 9.32 0.19	5 B 8.30 0.277	6 C 11.26 1.263	7 N 14.54 Unstable	8 O 13.61 1.461	9 F 17.42 3.401	10 Ne 21.56 Unstable
11 Na 5.14 0.548	12 Mg 7.64 Unstable	13 Al 5.98 0.441	14 Si 8.15 1.385	15 P 10.55 0.746	16 S 10.36 2.077	17 Cl 13.01 3.613	18 Ar 15.76 Unstable
19 K 4.34 0.501	20 Ca 6.11 0.0245	31 Ga 6.00 0.3	32 Ge 7.88 1.233	33 As 9.81 0.81	34 Se 9.75 2.021	35 Br 11.84 3.364	36 Kr 14.00 Unstable
37 Rb 4.18 0.486	38 Sr 5.69 0.052	49 In 5.78 0.3	50 Sn 7.34 1.112	51 Sb 8.64 1.07	52 Te 9.01 1.971	53 I 10.45 3.059	54 Xe 12.13 Unstable
55 Cs 3.89 0.4716	56 Ba 5.21 0.144	81 Tl 6.11 0.2	82 Pb 7.41 0.364	83 Bi 7.29 0.946	84 Po 8.43 1.9	85 At — 2.8	86 Rn 10.74 Unstable
87 Fr 4.0 0.46	88 Ra 5.3 0.100						* Meta-stable

III B	IV B	V.B	VI B	VII B	VIII B			I B	II B
21 Sc 6.56 0.188	22 Ti 6.83 0.079	23 V 6.74 0.525	24 Cr 6.76 0.666	25 Mn 7.43 Unstable	26 Fe 7.90 0.151	27 Co 7.86 0.662	28 Ni 7.63 1.156	29 Cu 7.72 1.235	30 Zn 9.39 Unstable
39 Y 6.50 0.307	40 Zr 6.95 0.426	41 Nb 6.77 0.893	42 Mo 7.16 0.746	43 Tc 7.28 0.55	44 Ru 7.36 1.05	45 Rh 7.46 1.137	46 Pd 8.33 0.557	47 Ag 7.57 1.302	48 Cd 8.99 Unstable
57 La 5.61 0.600	72 Hf 7.00 ≅ 0	73 Ta 7.88 0.322	74 W 7.98 0.815	75 Re 7.87 0.15	76 Os 8.70 1.10	77 Ir 9.00 1.565	78 Pt 8.96 2.128	79 Au 9.22 2.309	80 Hg 10.43 Unstable

Table 1: Electron affinities and ionization potentials of the elements in eV

In the present case of interest helium positive ions from a positive ion source, will undergo a double electron capture process to produce ions in the negative state.

The design is based on a so-called duoplasmatron positive ion source coupled to a charge-exchange canal. In this, positive He ions produced in the duoplasmatron ion source are extracted and directed to the charge-exchange canal where through atomic collisions with vapor molecules undergo double-electron capture and become negative. Subsequently, they are mass analyzed and injected into the EN 6 MV Tandem accelerator for acceleration. This method is particularly

promising for the production of those elemental negative ion species which are difficult to obtain by other methods **[HEI78].**

CHAPTER 2

GENERAL THEORY

2.1 INTRODUCTION

Negative ions can be formed through several processes, such as of dissociative attachment, charge transfer, volume production in plasmas, charge exchange, thermodynamic equilibrium, surface ionization and non-thermodynamic secondary surface ionization phenomena. A brief description of the technology of ion sources relevant to Tandem accelerators used to produce both positive and negative ions is given in this chapter. The choice of a suitable source depends on the beam requirements of the application, such as intensity, duty cycle and beam emittance.

2.2 NEGATIVE-ION PRODUCTION BY CHARGE TRANSFER

A small amount of negative ions are produced by charge transfer when a positive ion beam with an energy of 20 to 50 keV passes through a donor gas/vapor cell. If the donor gas is the same element as the positive ion, the charge transfer efficiency is as low as about 1%, but if an alkaline metal or an alkali earth metal is used as a charge transfer cell gas, the charge transfer efficiency increases to 10% or more **[WOL95]**

In such collisions it is possible that two electrons are shifted from the neutral particle to the positive ion through a charge transfers. Alkaline earth metals selected as the neutral particles because they easily release their electron. The efficiency of the charge transfer depends on

parameters such as the amount and type of vapor in the cell and the incoming ion energy. **[WOL95]**

2.3 CHARGE EXCHANGE PROCESSES

During collisions between an ion, neutral atom or molecule and another ion, neutral atom or molecule, an electron can be transferred from one of the colliding partners to the other with high probability. This process is highly depended on the collision energy, ionization potentials and electron affinities of the colliding partners. A single charge transfer is also referred as "charge exchange" or "electron capture". The charge transfer process can be described with respect to the energy defect ΔE involved in the transfer, as defined by the following interaction of the projectile X and target Y:

$$X^+ + Y \rightarrow X + Y^+ + \Delta E_1$$

Where; ΔE_1 is equal to the difference in ionization energies Ei of the colliding partners. For negative ion formation, the energetic neutral atom X must undergo a second collision, as represented by the following reaction:

$$X + Y \rightarrow X^- + Y^+ + \Delta E_2$$

where ΔE_2 is the difference between the electron affinity E_a of X and the ionization energy E_i of Y.

NWU LIBRARY

In general, the charge transfer collision takes place at relatively large impact parameters, in which the projectile scattering angle is small and the product ion is scattered nearly perpendicular to the impact momentum vector.

When the projectile velocity is low compared to the speed of the electrons in the target, the collision is called slow. In such collisions, the electrons have sufficient time to re-arrange themselves according to the changing positions of the nuclei. Thus if at any time during the collision the internuclear distance is sufficiently small for electron transfer to take place, this will happen with unit probability. Electron transfer cross sections for slow collisions are thus determined by the critical distance for transfer and are of the order of the geometrical size of the involved particle or larger.

In fast collision the speed of projectile is significantly larger than the typical speed of the electrons in the target. In this process very little time is available during the collision for the electrons to respond to the motion of the nuclei. However in this velocity range, electron transfer is possible for impact parameters smaller than the critical distance, although the lack of an efficient mechanism to accelerate an electron from the target system to the projectile system results in very small electron transfer probabilities. For these reasons, the cross sections for electron transfer process in fast collisions are much smaller than for slow collisions and decrease rapidly with increasing velocity **(STO05)**.

In order for an electron to be transferred in a fast collision, a mechanism must exist that accelerates the electron to a matching velocity. Different mechanisms exist and those relevant in this velocity regime are kinematic and double scattering processes (Thomas processes). The kinematic process can best be described as a single projectile-electron interaction in the field of

the target nucleus. In the quantum mechanical description of the target and projectile states there are high velocity tails of the electron wave function. Transfer is possible due to the overlap between these velocity tails **(SHA27)**. Hence capture is still possible, even though the projectile speed is much larger than the typical target electron speed. It is clear that this overlap, and consequently the cross section for this process, decreases very rapidly with the speed of the projectile **(STO05)**.

L.H Thomas in 1927 described in a classical picture with two binary collisions, very much like in figure 2.1. The process has a later also been described in a quantum mechanical framework. In this picture there is first an interaction between the projectile and the electron. In the collision the electron scatters in an angle of 60^{o} in the forward direction, a scattering in 60^{o} is the only binary collision where an electron with zero initial velocity can be accelerated to the same speed as the projectile. Because the target nucleus is much heavier than the electron, the speed of the electron relative to the nucleus will not change in the second interaction, where the electron gets a direction parallel to the projectile. Even though it is a two step process, it can be shown that the cross section for the process scales as v_p^{-11}, so it falls off less rapidly with the projectile velocity than first order kinematic capture. Since we know how much momentum that has to be exchanged between projectile and electron to give the electron the right direction, we can at the same time determine the projectile scattering angle. The angle is given by $\theta_{thomas} = \sqrt{3}/(2m_p)$ where mp is the projectile mass in atomic units. This angle is independent of the projectile velocity and equal to 0.47mrad for proton projectile.

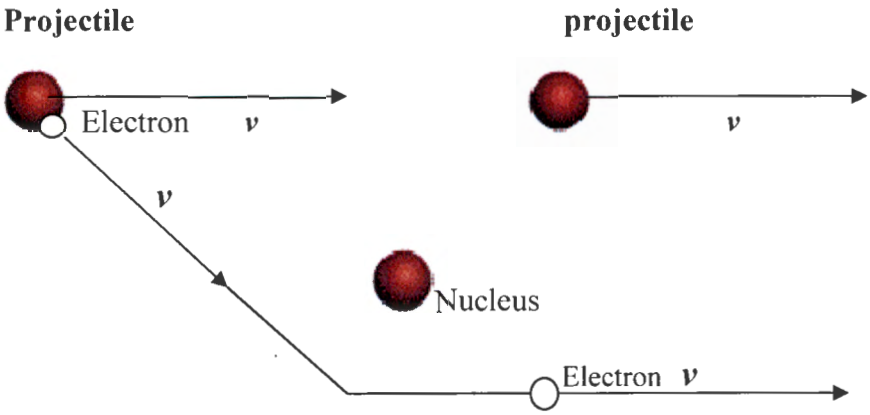

Figure 2.1: By scattering on the nucleus, the electron and the projectile continue on the same path.

Ever since the early days of quantum mechanics there has been high theoretical activity concerning this problem. Classical models have been considered to gain general insight into the transition mechanisms and dependencies on the collision parameters. A theoretical model based on classical mechanics was constructed by Thomas **[THO27].** The capture of a bound electron by a fast projectile was described as a double scattering event whereby the electron is first scattered off the projectile and then scattered elastically off the target nucleus. An electron which finally moves with the same velocity and in the same direction as the projectile is considered to be captured. This model predicts a velocity dependence of v_p^{-11} of the cross section. The Thomas scattering mechanism was observed experimentally by Horsdal-Pedersen *et al* **(HOR02)** and Vogt *et al* **(VOG86)** but generally plays only a minor role.

The case of interest in the present study lies within the regime of slow collision with projectile velocities less than the Bohr velocity ($V_{Bohr} = 2.19 \times 10^6 ms^{-1}$). A simple classical model valid for one-electron capture in a broad energy range (keV to MeV) applicable to slow and fast collisions was introduced by Bohr and Lindhard. In their model, they revealed that an electron can only be transferred if the Coulomb force exerted by the projectile exceeds the initial binding

force and if the electron's kinetic energy in the projectile frame is smaller than its potential energy. The model predicts an energy independent cross section at low impact energies.

2.4 BOHR AND LINDHARD MODEL

A first classical description of one-electron capture in collisions between highly charged ions and atomic targets was provided by Bohr and Lindhard **(BOH54)**. It has proven to give good estimations of the absolute cross sections and their dependencies on the impact energy, target electron binding energy and projectile charge state. Two distinctive ion–atom interaction distances are introduced. Firstly the electron can be released from the target nucleus when the projectile is close enough that its attractive Coulomb force is equal to the binding force of the electron in the atom, i.e.,

$$\frac{q}{R^2} = \frac{v_e^2}{a}$$

Where: v_e and a are the velocity of the electron and the radius of its orbital, respectively, as defined in the Bohr model. The release distance R_r is then given by:

$$R_r = \frac{\sqrt{qa}}{v_e}$$

Secondly, the electron can be captured if in the projectile frame its potential energy is larger than its kinetic energy. The distance at which this condition becomes valid is determined by

$$\frac{q}{R} = \frac{1}{2} v_p^2$$

and capture is possible for distances smaller than

$$R_c = \frac{2q}{v_p^2}$$

Which; is called the capture distance.

For $Rr < Rc$ the condition for capture is fulfilled and the cross section is given by

$$\sigma_{cap} = \pi R_r^2 = \pi \frac{qa}{v_e^2}$$

This means that for projectile velocities $v_p < v_{cr} = \sqrt{2v_e^2}\left(\frac{q}{a}\right)^{1/4}$, with v_{cr} the critical velocity defined by $R_r = R_c$, the capture cross section is independent of the impact energy. On the other hand for $R_r > R_c$ release can take place before capture is possible. If the release process would happen instantaneously, capture would not be possible and the cross section would become zero. However, the release takes a finite amount of time while the projectile is passing the target, and takes place only with a probability per unit time of the order of v_e/a. Therefore there is a chance that the electron is still at the target when the internuclear distance has decreased below the capture distance. The probability of electron release within a distance R_c is on the order of $\left(R_c/v_p\right)\left(v_e/a\right)$ Thus for $R_r > R_c$ the cross section is

$$\sigma_{cap} = \pi R_c^2 \left(\frac{v_e}{a}\frac{R_c}{v_p}\right) = 8\pi q^3 \frac{v_e}{a} v_p^{-7}$$

meaning that for projectile velocities $v_p > v_{cr}$ the capture cross section decreases very strongly with increasing projectile velocity as v_p^{-7}. The two cross section regions do not match at $v_p = v_{cr}$ if the factor $\left(R_c/v_p\right)\left(v_e/a\right)$ is not equal to one. In figure 2.2 Bohr-Lindhard cross sections are shown for one-electron capture from Na(3*s*) by H^+, He^{2+} and O^{6+} projectiles. Also a comparison between capture from Na (3*s*) and Na*(3*p*) by O^{6+} is made. The velocity of the target electron v_e is calculated from the relation with the ionization potential *I*, namely $v_e = \sqrt{2I}$. For the orbital radius *a* the $\langle 1/r \rangle^{-1} = n^2/Z_{eff}$ expectation values of the radial probability densities are taken, using hydrogenic wave functions with an effective nuclear charge. This yields for Na (3*s*) *a* = 4:9 a.u. (Z_{eff} = 1:84) and for Na*(3*p*) *a* = 6:3 a.u. (Z_{eff} = 1:42).

Considering single ionization we can already make the observation that according to the Bohr-Lindhard model ionization has a threshold at $v_p = v_{cr}$, under the assumption that ionization can only occur for $R < R_r$. For lower velocities capture is 100% efficient because the second condition, $R_r < R_c$, is always fulfilled. However for higher velocities ionization becomes possible, if we interpret the situation that an electron is released but not captured as an ionization event. Bohr obtained an analytical expression for the ionization cross section, based on the Rutherford cross section for energy transfer to a free, stationary electron. Ionization occurs when the energy transferred exceeds the ionization potential. Therefore the ionization cross section is obtained by the integration of the Rutherford cross section from the ionization potential *I* to the maximum transferable energy $2v_p^2$ and found to be:

$$\sigma_{ion} = 4\pi q^2 v_p^{-2}\left[(2I)^{-1} - (2v_p)^{-2}\right]$$

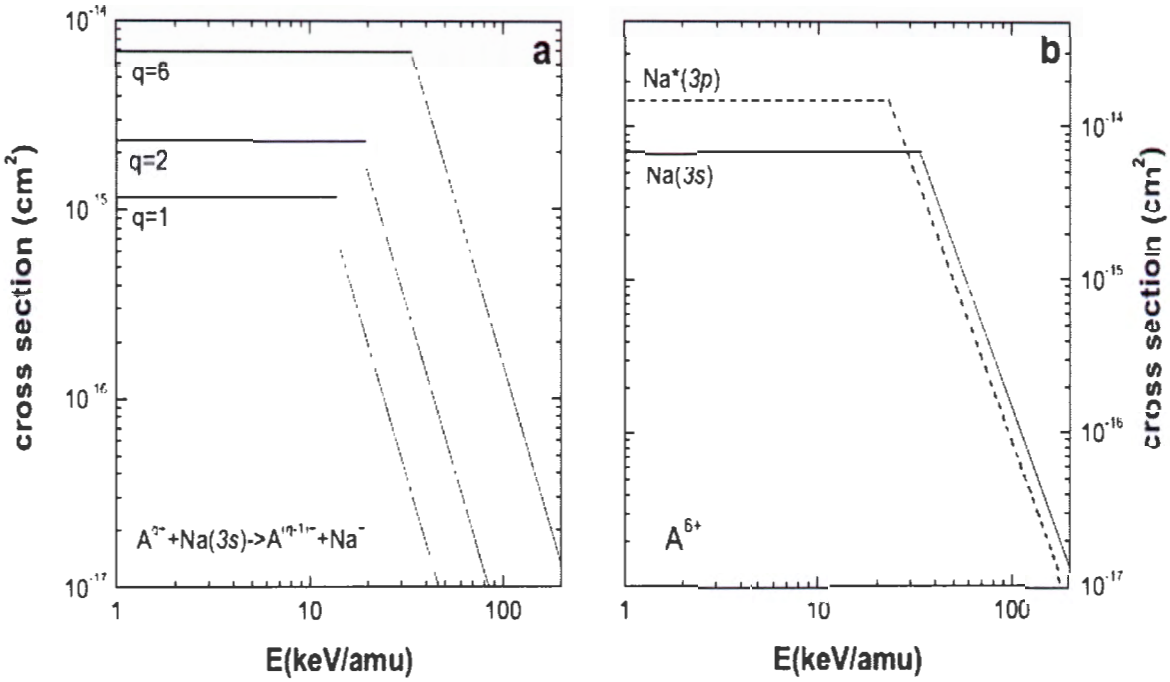

Figure 2.2: One-electron capture cross sections for collisions on Na according to the Bohr-Lindhard model (a) for different projectile charge states and (b) target binding energies.

2.5 ELECTRON CAPTURE TO THE CONTINUUM OF NEUTRAL PROJECTILES

The discussion regarding the second electron capture by the now neutral projectile to form a negative ion metastable state is based on the association to the observed cusp-shaped peak **[SAR89]** of electron emission centered at electronic velocities equal to the projectile's. The cusp-peak electron emission cross-section is associated in this way directly with electron capture to the continuum of neutral projectiles.

In an ab initio theoretical calculation by [**BAR90**], adopting a final state interaction approach, the double-differential cross-section was estimated as an enhancement factor multiplying the corresponding first Born approximation. In this manner, a Lorentzian peak centered at an electronic velocity equal to that of the incident projectile is desired in accordance to experimental observations.

A brief description of the above theoretical model follows:

$$P + T \rightarrow P + T^{+} + e^{-}$$

where P is the projectile and T is the target.

In the centre of mass system co-ordinates are defined as: r_T, r_P = position vectors of e^- relative to target and projectile.

R_T= co-ordinates of P relative to centre of mass of $e^- + T$.

R_P= co-ordinates of T relative to centre of mass of $e^- + P$.

$$r_T = \beta r_P + R_P \qquad , R_T = -(1 - \alpha\beta) r_P + \alpha R_P$$

and

$$r_P = \alpha r_T - R_T \qquad , R_P = (1 - \alpha\beta) r_T + \beta R_T$$

with

$$\alpha = \frac{M_T}{1+M_T} \qquad , \beta = \frac{M_P}{1+M_P}$$

In the momentum space:

$$k_T = \alpha k_p + (1-\alpha\beta)K_P \qquad , K_T = -k_P + \beta K_P$$

and

$$k_P = \beta k_T - (1-\alpha\beta)K_T \qquad , K_P = k_T + \alpha K_T$$

The transition matrix element for $P + T \rightarrow P + T^+ + e^-$ is as follows:

$$t_{fi} = \left\langle \psi_f^- \middle| V_P \middle| K_i, \phi_{Ti}, \phi_{Pi} \right\rangle$$

where:

V_P= short-range electron-projectile interaction,

$\left| K_i, \phi_{Ti}, \phi_{Pi} \right\rangle$ = initial state with bound states ϕ_{Pi} and ϕ_{Ti}

According to the final state theory **[GILL64, TAY72]** the transition matrix for small values of k_P can be approximated by

$$t_{fi} = \frac{1}{f_0^*(k_P)} t_{fi}^B$$

with

$t_{fi}^{B} = \left\langle K_f, \psi_{kT}^{-}, \phi_{pf} \middle| V_P \middle| K_i, \phi_{Ti}, \phi_{Pi} \right\rangle$ = to the first Born Approximation transition matrix for the ionization of the target.

$f_0(k_P)$ is the so-called s-wave Jost function

$$\frac{1}{f_0(k)} = (2\pi)^{3/2} \psi_k^{+}(r=0)$$

Introducing V_P as,

$$V_P = \sum_{j=1}^{Z_P} \frac{1}{|r_P - r_j|} - \frac{Z_P}{r_P}$$

the transition matrix t_{fi} becomes,

$$t_{fi} \cong \frac{1}{f^*(k_P)} \frac{1}{2\pi^2 Q^2} \left[\left\langle \phi_{pf} \middle| \sum_{j=1}^{Z_P} e^{-iQ.rj} \middle| \phi_{Pi} \right\rangle - Z_P \left\langle \phi_{pf} \middle| \phi_{pi} \right\rangle \right] \left\langle \psi_{kT}^{-} \middle| e^{i\alpha Q.r_T} \middle| \phi_{Ti} \right\rangle$$

With

$Q = K_i - K_f$ the momentum transfer.

Substituting in the double differential cross section

$$\frac{d\sigma}{dk_T} = \frac{(2\pi)^4}{K_i} \int |t_{fi}|^2 \delta(E_f - E_i) dk_T$$

$$= \frac{(2\pi)^4}{v_i} \int |t_{fi}|^2 \delta\left[\frac{Q^2}{2\mu} - Q.v_i + \left(\frac{k_T^2}{2\alpha} - \sum_{Ti}\right) + \left(\sum_{Pf} - \sum_{Pi}\right)\right] dQ$$

and neglecting terms of order $1/M$, we find that the Jost function can be factorized from the cross section, the above equation, to give

$$\frac{d\sigma}{dk_T} = \frac{1}{|f_0(v')|^2} \frac{d\sigma^B}{dk_T}$$

With

the first-order Born double differential cross section (DDCS) for the ionization of the target.

$$Q_0 = \frac{1}{v_i}\left[\frac{k_T^2 + Z_1^2}{2\alpha} + \left(\sum_{Pf} - \sum_{Pi}\right)\right]$$

is the minimum momentum transfer. Z_1 is the ionisation charge of the target, and $v_i = K_i/\mu$ is the initial velocity of the projectile. $v' = k_T - v_i$ is the velocity of the electron in the projectile frame. In order to extend the singe ionisation of monoelectronic targets to the multielectronic case, an independent-electron model is assumed **[SAL72, FAI88]**. Therefore the DDCS has been multiplied by the number Ni of the target electrons with binding energy $Z_1^2/2$.

For a fully stripped projectile of charge Z_p the s-wave Jost function is:

$$f_0(v') = \frac{e^{-\pi Z_p/2v'}}{\Gamma(1 - iZ_p/v')}$$

NWU LIBRARY

where v' is the velocity acquired by the ejected electrons in a mean-binary encounter with the projectile given by $v' \cong v_i\left[1-2\alpha\left(\sum_{Pf}-\sum_{Pi}-\sum_{Ti}\right)/v_i^2\right]^{1/2}$

The cross-section therefore becomes

$$\frac{1}{|f_0(v')|^2}=\frac{2\pi Z_p/v'}{1-\exp\left(-2\pi Z_p/v'\right)}$$

For a neutral projectile now, the s-wave Jost function becomes, **[BAR90]**

$$f_0(v')\propto\frac{1+ia v'}{a}$$

with a, the s-wave scattering length for the electron-projectile interaction and the cross section becomes:

$$\frac{1}{|f_0(v')|^2}\propto\frac{a^2}{1+a^2v'^2}$$

CHAPTER 3

PRODUCTION OF NEGATIVE HELIUM IONS

3.1 METASTABLE NEGATIVE IONS

Metastable ions are an important class of negative ions that can be formed in exited states of the parent atom and live long enough to be useful. In order to induce electron attachment and thus form such metastable states, it is necessary to form the particular excited electronic state of the neutral atom to which an electron can be attached. The charge transfer process is suitable for metastable ion formation.

They are long lived states that are dipole- forbidden from decaying to the ground state. In comparison to ground state atoms, metastable atoms have much larger cross sections; they also have a lot of internal energy. Since they are long lived, substantial populations of metastable atoms can form in many plasmas. Negative helium ion (He^-) is one of the classical examples of metastable atoms with high probability in the ^4P state through sequential charge exchange with a low ionization-potential charge exchange vapor.

Negative helium ions are negative particles where an electron is attached to a neutral particle that is not in its ground state. It has a lifetime of 18.2 microseconds. It is believed that during the formation of this particle the neutral helium atom becomes trapped in an excited triplet state whose decay to the ground state cannot take place without an electron spin flip **[KEN73].** During this period, while the neutral helium is excited, a third electron can be attracted to the atom and be bound to form a negative ion.

Helium has two metastable states, the 2^1S and the 2^3S. As illustrated in figure 3 (the energy level diagram) below, they both lie about 20eV above the ground state.

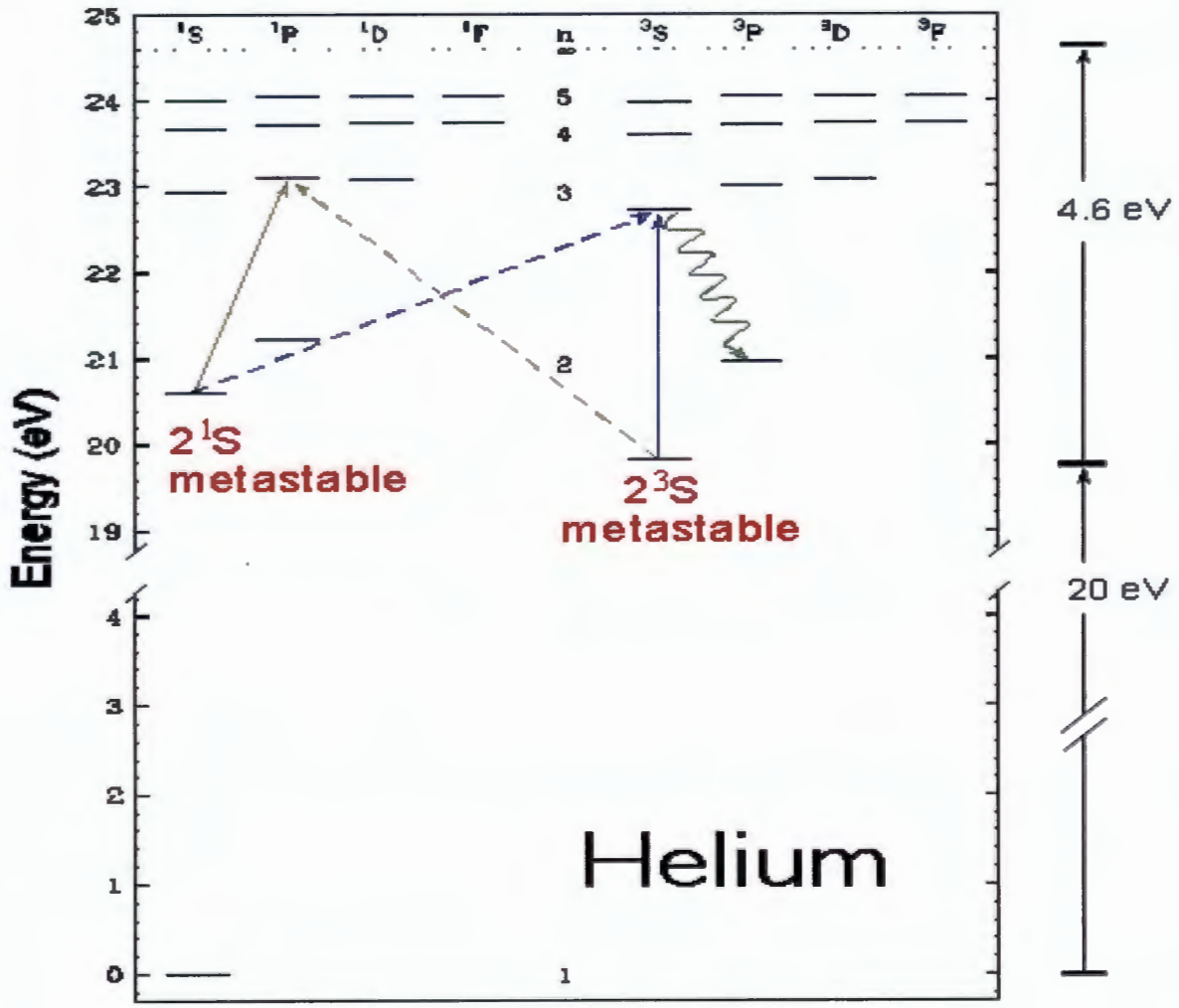

Figure 3: Energy level diagram illustrating helium's metastable states **[WWW3]**

3.2 HELIUM ENERGY LEVEL

The helium ground state consists of two identical 1s electron. The energy required to remove one of them is the highest ionization energy of any atom in the periodic table: 24.6electron volts. The energy required to remove the second electron is 54.4eV, as would be expected by modeling it

after the hydrogen energy levels. ion is like a hydrogen atom with two units of charge in the nucleus. Since the hydrogenic energy levels depend upon the square of the nuclear charge, the energy of the remaining helium electron should be just 4 ×(-13.6eV) = 54.4eV as observed.

The fact that the second electron is less tightly bound can be interpreted as a shielding effect; the other partly shields the second electron from the full charge of the nucleus. Its energy can be used to model the effective shielding as follows:

First electron $-54.4\text{eV} = Z^2 \quad (-13.6\text{eV}); \qquad Z = 2$

Second electron $-24.6\ \text{eV} = Z^2_{\text{eff}} \quad (-13.6\text{eV}); \qquad Z_{\text{eff}} = 1.34$

Another way to view the energy is to say that the repulsion of the electrons contributes a positive potential energy which partially offsets the negative potential energy contributed by the attractive electric force of the nuclear charge. The description of any electron in a multi electro atom must find a way to characterize the effect of the other electrons on the energy **[WWW3]**.

3.3 PRODUCTION OF NEGATIVE HELIUM IONS

For a long time the principal method of obtaining He^- ions has been the transformation of positive helium ions () in various permanent gases such as (He, Ne, Ar, Kr, O_2, H_2 and N_2) unfortunately, in such collisions the cross section for production of He^- is small and of the order of 10^{-19} or 10^{-20} cm^2 **[KEN73].** He^- ion source operating on this principle has a low intensity

[D'YA71]. The commonly used medium for such charge exchange has been hydrogen. In this process, the positive ions are produced by commercially available ion source and are accelerated to an optimum energy for passage through the charge exchange medium. The voltage to which the ions are accelerated is determinative of the energy of the resulting negative ions. Although hydrogen was satisfactory for a fairly wide range of negative ions it was very poor for He^- enabling only about $2x10^{-4}$ of the positive ion beam to be converted to negative ions and even then at inconveniently high exchange voltage **[DON67]**.

The energy at which this maximum yield occurs is 140 keV for H_2 and is within a factor of two of this energy for the other gases. The high energy of the He^- obtained from the collisions mentioned above is a serious disadvantage in atomic physics studies and the low yield makes it difficult to get adequate intensities for either nuclear physics or atomic physics experiments (**[DON67**).

The processes for producing He^- ions from positive ions, which the maximum yield is higher than that of the process reported above has been developed by Donally et al and Middleton et al **[MID71, DON67]**. These exchange processes have been studied extensively because of their applications to controlled thermonuclear research and tandem accelerators **[HEI78.1]**.

Charge exchange of an initially positive ion beam in an electron donor target is one way of producing negative beams. Metal vapor charge exchange targets have been extensively used since the appearance of Donnally and Thoeming paper **[DON67]** on He^- production by charge exchange. They recognized the importance of projectile-target combination with minimum energy defect in two separate electron capture processes in the stepwise formation of negative helium ions from positive ones **[HEI78.1]**.

3.3.1 TWO STEP PROCESS FOR PRODUCING He^-

The observation of the negative helium in an electric discharge of helium atoms can be explained in the following way. By a relatively small electrical discharge the helium atom becomes excited into the lowest triplet state (1s2s) ^2S and remains in this metastable state for a while (Lifetime about 10^{-8} sec). If now the binding energy calculated for the negative ion in the $^4P_{5/2}$ is lower than the actual (experimental) energy of the lowest triplet state of the neutral atom, one extra electron can be attached in a 2p orbital of the atom, hence the formation of negative ions. It remains in the metastable state until collision of the second kind, i.e., collision with neighboring particles, causing the ion to give up its extra energy without radiation.

Donnally et al **[DON67]** suggested that negative helium ions could be produced by a nearly-resonant two-step charge exchange reaction, as follows:

(i) Formation of He^0 (1s 2s) $^3S_1$ from (1s) by a charge exchange transfer collision with an alkali atom;

(ii) Formation of He^- from He^0 (1s 2s) $^3S_1$ by pick-up of a 2p electron :

This experiment uses charge exchange between helium ions and alkali vapor to produce metastable atoms:

$$+ X \rightarrow He^* + X^+$$

Where X is any alkali metal;

This process yields a target with more metastable atoms than ground state atoms. Thus, measurements can be taken at much higher electron energies (up to 1500eV). To get around the problem of excitation out of the ground state, it would be nice to have a target composed only (or

at least mostly) of metastable atoms. One way of achieving this goal is through near resonant charge exchange.

$$+ X \rightarrow He^0 (1s\ 2s)\ ^3S_1 + X^+ \qquad (1)$$

Where X is any alkali metal;

The ground state binding energy of any alkali metal is almost the same as the binding energy of the He (2^1S) and He (2^3S) levels. Thus, in a collision between a helium ion and an alkali atom, there is large cross section for charge exchange into the metastable levels (small energy defect ~0.5eV), while the cross section for charge exchange directly into the ground state is very small (large energy defect ~20eV)

$+ X \rightarrow He\ (2^3S) + X^+$ (Energy defect ~ 0.5eV)

$+ X \rightarrow He\ (2^1S) + X^+$

$+ X \rightarrow He\ (1^1S) + X^+$ (Energy defect ~ 20eV)

$$He^0 (1s\ 2s)\ ^3S_1 + X^0 \rightarrow He^-\ (1s\ 2s\ 2p)\ ^4P_{5/2} + X^+ \qquad (2)$$

Processes (1) and (2) will have a larger cross section if the charge exchange target X is an element with a small ionization potential, an alkali metal. In this case process (1) will be almost a resonant charge transfer of ions into the excited state He^0 (1s 2s) $^3S_1$, and the charge exchange cross section will increase with decreasing resonant defect $|\Delta E|$ of process (1): in this case one has to take into account the fact that the charge exchange cross section depends on the atomic number of the target. The cross section for process (2) also should increase with decreasing

resonance defect; this is confirmed by the larger yield for metallic than for gaseous charge exchange target **([D'YA71].** The process proceeds via the metastable ^3S state rather than the ground state because the electron configuration in the metastable atom matches that of the inner electrons in the negative ions **[HOO80].**

Because the production of negative helium ions is probably a two-stage reaction, the individual cross sections for both neutralization and electron addition must be high **[KEN73].** An important point which Donnally made was that if in the electron addition stage the charge exchange atom for helium is chosen such that for large inter-nuclear separations the potential energy curve of $He^- + A^+$ is just a few eV above the potential energy curve for the neutral combination $He^{0,} + A^0$ then the Coulomb interaction will tend to bring these potential energy curves together as the internuclear separation decreases with the possibility of mixing and crossing present. When this condition is satisfied, the Massey criterion suggests that the cross sections for exchange can be large. This argument implies that a suitable charge exchange molecule should have an ionization energy which is only slightly greater than the electron affinity of the final electron in the negative ion [**KEN73**].

Holoien and Midtdal calculated that the (1s 2s 2p) ^{4} $^4P_{5/2}$ state of He^- i s metastable against auto-ionization with an estimated mean life of $1.7x10^{-3}$ sec which is a generous time to be observed in beam experiments [**DON67**]. In this $^4P_{5/2}$ state, the binding energy of the 2p electron is of the order o f 0.075 eV and all the other possible states of He^- undergo decay by auto- ionization, i.e., decay by emission of a free electron. Szanto de Toledo et al [**SZA77**] observed, in support of this, that even a trace of cesium vapor first causes almost 100% conversion of to He^0, but only after the cesium vapor pressure is further increased, the yield of He^- decreases, probably because of the increasing importance of triple collision.

Lorentz et al found the total charge transfer cross section for - Cs collision to be 1.66 $X10^{-14}$ cm^2 at energy of 2keV.They point out that this very large cross section is probably due to the nearly resonant charge transfer to excited state of He **[LOR65].**

Middleton et al also provides a process for producing large species of negative helium ions utilizing metallic vapor. Experiments performed utilizing the process of this invention have determined that high energy beams of negative helium ions can be produced by charge exchange in a wide variety of vapors in addition to those of the alkali metal **[MID71].** In particular the vapors of alkaline earth metal are very effective; they have sufficient reducing power to form negative helium ions. The vapor properties which appears to be most determinative of the efficiency of the production of beams of negative helium and other ions are that, the vapor be metallic and have a low ionization potential. In general the lower the ionization potential the greater is the yield of the negative ions. In addition it is desirable that the vapor should be constituted of atom having a low atomic number in order to minimize the multiple scattering of the ion beam which results from collisions with the vapor atoms **[MID71].**

While the process has been described in terms of vapors comprised of metallic atoms, beams of negative ion can be produced at desirable energies by charge exchange in the vapors of other low ionization potential elements, as well as compound vapors. It is anticipated that any compound having low ionization potential or a compound containing atoms having a low ionization potential which would be released upon collision would be a suitable vapor medium **[MID71].**

The use of high voltages and correspondingly high charge exchange energies plays a dual role in the process of this invention. Higher energies are required to effect charge exchange e.g., in using the vapor of lithium for charge exchange medium intense beams of negative ^3He were

produced at an exchange energy of ~20 keV and slightly higher yield of ^{4}He at an exchange energy of ~26 KeV **[MID71].**

The second beneficial role played by using high exchange energies is that the resulting negative ions are produced at higher energies. This is of critical importance in the operation of a Tandem accelerator where the negative ions must be introduced at higher energy in order to avoid beam scattering preferably approaching 100KeV. Production efficiency of the He^- beam is largely determined from the double charge exchange efficiency while the efficiency is strongly affected by beam energy. The process of this invention is general in that, it is not restricted to the production of negative helium ions. Rather, a whole range of negative ions can be produced by charge exchange in a vapor medium possessing a low ionization potential.

It appears that He is very unique in that its negative ions can only be formed by charge exchange, generally in vapor of alkali metals. These elements are easier to handle due to their high vapor and simple chemical behavior, their low ionization potential has permitted many laboratories to produce element –selective beams very efficiently.

From the above discussions about negative helium ions formation processes, a nearly-resonant two-step charge exchange reaction will be considered for the present application as it agrees well with the Bohr-Lindhard model presented in chapter 2.

CHAPTER 4

BEAM TRANSPORT ELEMENTS

4.1 INTRODUCTION

During the design of a beamline for the transport of charged particles, the characteristics of the transport elements, which are used to focus and direct the beam to the desired location, together with their matrix representations, have to be calculated. The calculations are iteratively repeated until the desired beam characteristics, as specified by the user, without any losses of beam along the beamline are obtained. A beam of charged particles that traverses a drift space spread out horizontally ad vertically. Dipole magnets are used to direct and change the beam direction. The matrices of the beam elements that transport charged particles are explained below [**MAI02**].

4.2 DRIFT SPACES

A drift space is a field-free region in the beamline through which the beam passes and it is has only one parameter, L, its length. As a ray traverse a drift space, its final co-ordinates are given in terms of its initial co-ordinates as:

$$x_f = x_i + L\theta_i \,, \qquad y_f = y_i + L\phi_i \tag{4.1}$$

where: x_f is the final particle displacement in the x-direction

y_f Is the final displacement in the y direction,

x_i is the initial displacement in the x-direction

y_i is the initial displacement in the y-direction,

θ_i is the angular divergence in the x-direction and

ϕ_i is the initial angular divergence in the y- direction.

For six dimensional phase space the first order transfer matrix for a drift space is as follows

$$R=\begin{bmatrix} 1 & L & 0 & 0 & 0 & 0 \\ 0 & 1 & 0 & 0 & 0 & 0 \\ 0 & 0 & 1 & L & 0 & 0 \\ 0 & 0 & 0 & 1 & 0 & 0 \\ 0 & 0 & 0 & 0 & 1 & L/y^2 \\ 0 & 0 & 0 & 0 & 0 & 1 \end{bmatrix} \quad (4.2)$$

Where

L is the length of the drift space,

$$\frac{1}{\gamma^2} = 1 - \frac{v^2}{c^2}$$

v is the speed of the particles and

c is the speed of light in vacuum

NWU LIBRARY

4.3 DIPOLE MAGNETS

The first order transfer matrix for a dipole magnet is given by equation (4.3) **[MAI02]:**

$$R = \begin{bmatrix} \cos k_x L & \frac{1}{k_x}\sin k_x L & 0 & 0 & 0 & \frac{1}{\rho k_x^2}(1-\cos k_x L) \\ -k_x \sin k_x L & \cos k_x L & 0 & 0 & 0 & \frac{1}{\rho}\sin k_x L \\ 0 & 0 & \cos k_y L & \frac{1}{k_y}\sin k_y L & 0 & 0 \\ 0 & 0 & -k_y \sin k_y L & \cos k_y L & 0 & 0 \\ -\frac{1}{\rho}\sin k_x L & -\frac{1}{\rho k_x^2}(1-\cos k_x L) & 0 & 0 & 1 & -\frac{1}{\rho^2 k_x^3}(k_x L - \sin k_x L) + \frac{L}{\gamma^2} \\ 0 & 0 & 0 & 0 & 0 & 1 \end{bmatrix} \quad (4.3)$$

where, $k_x^2 = \frac{1-n}{\rho^2}$, $k_y^2 = nh^2$

ρ is the radius of curvature of the central trajectory,

L the path length of the central orbit,

n the normalized gradient of the bending magnet (dimensionless),

h the curvature of the central trajectory and

γ the relativistic factor

The transfer matrix transforms the six co-ordinates of each particle in the beam that passes through the bending magnet from its entrance to the exit. The following figure shows the magnetic field boundaries of a dipole, bending magnet, where R_1 and R_2 are the radii of curvature of the entrance and exit faces of the bending magnet, respectively.

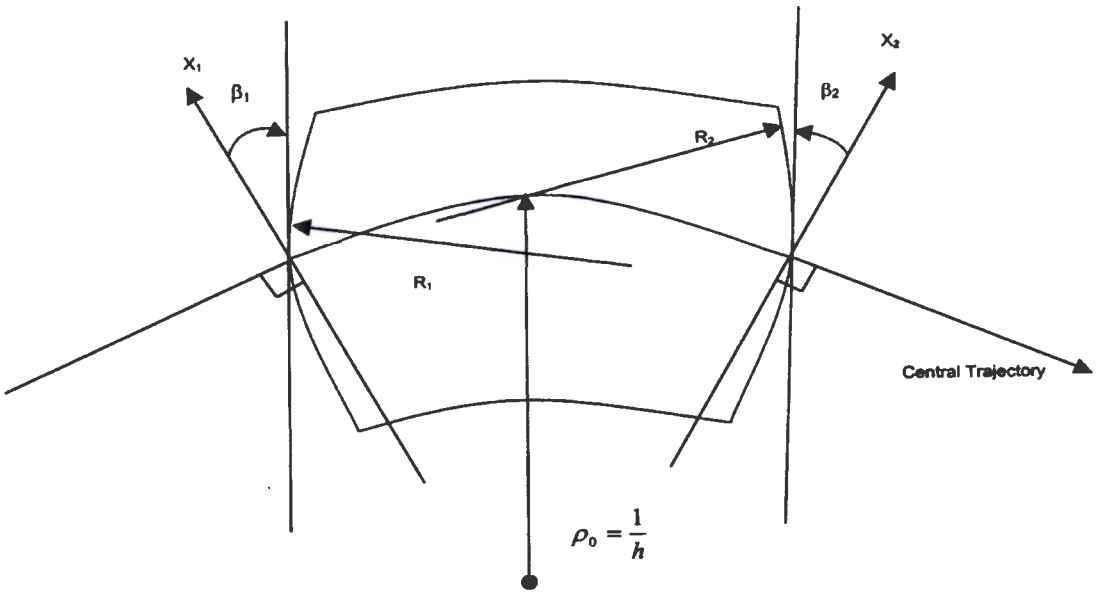

Figure 4.1: Magnetic field boundaries of a bending magnet and the entrance, β1, and exit, β2, pole face rotation angles of the beam.

The pole faces are the surface of the magnet that faces the incoming beam (entrance pole face) and the beam where it leaves the magnet (exit pole face). Both the entrance and exit pole face rotation angles are used with bending magnets. The pole face rotation angles describes the deviation of the normal vector for a given pole face with respect to the incident or exit reference trajectory direction. The pole face rotation angles can be used to adjust the magnet field path integral for the off- axis particles, in order to achieve different focusing conditions for those particles. The sign conventions for x, β, R and h, as shown in the figure 4.1, are all positive. The positive y direction is out of paper. Positive β-values imply transverse focusing. Positive R-values (convex curvature) of the magnet edge introduces negative sextupole components of strength $S = \left(-h/2R\right)\sec^3\beta$. **[MAI02]**

$$\mathbf{R}=\begin{bmatrix} 1 & 0 & 0 & 0 & 0 & 0 \\ \frac{\tan\beta}{\rho_0} & 1 & 0 & 0 & 0 & 0 \\ 0 & 0 & 1 & 0 & 0 & 0 \\ 0 & 0 & -\frac{\tan(\beta-\psi)}{\rho_0} & 1 & 0 & 0 \\ 0 & 0 & 0 & 0 & 1 & 0 \\ 0 & 0 & 0 & 0 & 0 & 1 \end{bmatrix}$$

where,

ρ_0 is the radius of curvature of the central orbit,

B the angle of rotation of the pole-face and

ψ a correction term resulting from the finite extent of the fringing fields.

CHAPTER 5

BEAM TRANSPORT FORMALISM

5.1 INTRODUCTION

The transport of charged particle beams under high vacuum conditions requires the use of electrostatic and electromagnetic methods to ensure transmission over large distances under different physical conditions. Such electromagnetic "optical" elements act as focusing lenses or bending and steering devices, for example dipole magnets are employed for changing the beam direction but also contribute to the focusing of the beam, while a set of electrostatic cylinder, Einzel lenses can act as focusing elements.

The beam optical elements and charged particles are represented by matrices. For the design of beamlines, it is convenient to consider the behavior of the beam in a space in which all possible states of a system are represented known as the phase space, in addition to the dimensions and position of the beam in the laboratory space. For this purpose the computer program TRANSPORT is used, though the presented program is old-timers, its modernized version is still very useful for today's beam optics problems. In TRANSPORT, a beamline is described as a sequence of optical elements; such as dipole magnets drift spaces and Einzel lenses. Precise description of the beam parameters, such as ion type, charge, energy and emittance are required for a reasonably accurate calculation of the so called "beam envelope" as well as the description of the physical parameters characteristic of the various optical elements such as magnetic fields, magnet radius, pole faces, electrical fields and physical sizes of lenses.

TRANSPORT is a general matrix evaluation and fitting program. It can evaluate various matrices which represent the transmission of particles through a beam line, and vary physical parameters of the beam line to fit elements of such matrices to desired optimum values. **[CAR81]**. It is a first and second order matrix multiplication computer program intended for the design of static-magnetic beam transport system. **[BRO77]**

TRANSPORT considers a beamline to be comprised of a set of magnetic elements placed sequentially at intervals along an assumed reference trajectory. The reference trajectory is taken to be a path of a charged particle passing through idealized magnets (no fringing fields) and having the central design momentum of the beam line. Therefore, through a bending magnet, the reference trajectory is the arc of a circle, while through all other magnetic elements it is a straight line. The input data to TRANSPORT contain the initial floor coordinates and the direction of the reference trajectory, and the sequence of elements comprising the beam line. The elements include both drift spaces and magnetic elements, which are specified by their lengths, magnetic fields, and other relevant quantities. TRANSPORT can then calculate the floor coordinates of the reference trajectory at the interface between any two elements.

The program TRANSPORT will step through the beam line, element by element, calculating the properties of the beam or other quantities. One of the first elements is a specification of the phase space region occupied by the beam entering the system. Magnets and intervening spaces and other elements then follow in the sequence in which they occur in the beam line. Specifications of calculations to be done or of configurations other than normal are placed in the same sequence, at the point where their effect is to be made.

5.2 BEAM OPTICS AND TRANSPORT FORMALISM

For a particle with charge q, mass m and velocity v moving perpendicular to a uniform, magnetic field, B, on a circular orbit with radius of curvature, ρ, the Lorentz force is equal to the centrifugal force:

$$qvB = \frac{mv^2}{\rho},$$

$$\rho = \frac{mv}{qB}$$

From the above equation (4.1) it follows that the momentum, mv, can, for a given charge q, be expressed as the product of $qB\rho$. The product $B\rho$ is called the magnetic rigidity of the particle and is directly proportional to the particle's momentum. The expression relating the total energy E and the momentum ρ of a particle is: **[MAI02]**

$$E^2 = p^2c^2 + m_0{}^2c^2$$

with m_0 the rest mass of the particle.

The magnetic rigidity is given by:

$$B\rho = \frac{mv}{q},$$

$$= \frac{Ev}{qc^2},$$

$$= \frac{E}{qc}\beta$$

$$= \frac{E}{qc}\frac{1}{\gamma}\sqrt{\gamma^2 - 1}$$

$$= \frac{E}{qc}\frac{\sqrt{E^2 - E_o^{\,2}}}{E},$$

$$= \frac{\sqrt{E^2{}_k + 2E_0E_k}}{qc}$$

where:

$$\gamma = \frac{E}{E_0} = \frac{1}{\sqrt{1-\beta^2}},$$

$$\beta = \frac{v}{c}$$

c is the speed of light in a vacuum,

v the velocity of the particle,

E_0 the rest energy of the particle and

E_k the kinetic energy of the particle.

At any specified position in a beam line an arbitrary charged particle may be represented by a vector (single column matrix) X, in phase space whose components are the positions, angles, and momentum of the particle with respect to the reference trajectory.

The vector X describes the coordinates of a particle at a given position along the beam line and is made up as follows:

$$X = \begin{bmatrix} x_1 \\ x_2 \\ x_3 \\ x_4 \\ x_5 \\ x_6 \end{bmatrix} = \begin{bmatrix} x \\ \theta \\ y \\ \phi \\ \ell \\ \delta \end{bmatrix} \tag{5.1}$$

Where:

x is the horizontal displacement of the particle from the central axis of the beam,

θ is the angle of the particle trajectory in the horizontal plane,

y is the vertical displacement of the particle from the central axis of the beam,

ϕ is the angle of the particle trajectory in the vertical plane,

ℓ is the difference in the path length of the particle and that of the reference particle,

δ is the fractional momentum deviation of the particle $\left(\Delta p / p\right)$ with respect to the reference particle.

The value of this vector at any location in the beam line may be determined from its initial value by means of transfer matrix **R**, so that

$$X_1 = RX_0 \tag{5.2}$$

NWU LIBRARY

Where X_0 is the initial location and X_1 is the point of interest of the particle under consideration. The six by six matrix **R** takes on a simple form if the system has midplane symmetry, where all the magnetic potentials are odd in the vertical coordinate. Then we have

$$\mathbf{R}=\begin{bmatrix} R_{11} & R_{12} & 0 & 0 & 0 & R_{16} \\ R_{21} & R_{22} & 0 & 0 & 0 & R_{26} \\ 0 & 0 & R_{33} & R_{34} & 0 & 0 \\ 0 & 0 & R_{43} & R_{44} & 0 & 0 \\ R_{51} & R_{52} & 0 & 0 & 1 & R_{56} \\ 0 & 0 & 0 & 0 & 0 & 1 \end{bmatrix} \tag{5.3}$$

For static magnetic elements, whether or not we have midplane symmetry, all entries in the fifth column, except the fifth, and all entries in the sixth row, except the sixth, will be zero. Thus nothing affects the momentum, and the longitudinal separation affects no transverse coordinate.

The zero elements R_{13}, R_{14}, R_{23}, R_{24}, R_{31}, R_{32}, R_{41}, R_{42}, R_{36} and R_{46} in the R matrix result from a midplane symmetry of the magnetic field. The zero elements R_{15}, R_{25}, R_{35}, R_{45} and R_{65} results from the fact that the variables x, θ, y, ϕ and δ are independent of the path length difference, Because of the static magnetic field. The zeros of R_{61}, R_{62}, R_{63}, R_{64} and R_{65} are due to the fact that the momentum is a constant of motion and the field is time-independent **[MAI02]**. Whilst the zeros of R_{53} and R_{54} results from the fact that ℓ and the (y, ϕ) plane are decoupled.

Because of the midplane symmetry, the co-ordinates (x, θ) and (y, ϕ) are always orthogonal. Other non-zero matrix elements can be explained by inspecting their dimensions, that is

$$R_{11} = \left(x_n / x_0 \right)$$
$$R_{33} = \left(y_n / y_0 \right)$$
} transverse linear magnification

$$R_{22} = \left(\theta_n / \theta_0 \right)$$
$$R_{44} = \left(\phi_n / \phi_0 \right)$$
} angular magnification

$$R_{21} = \left(\theta_n / x_0 \right)$$
$$R_{43} = \left(\phi_n / y_0 \right)$$
} have dimensions of $1/L$ and is the inverse of the focal length

$$R_{12} = \left(x_n / \theta_0 \right)$$
$$R_{34} = \left(y_n / \phi_0 \right)$$
} have dimension of L and represent effective drift lengths through the system

$$R_{16} = \left(x_n / \delta_0 \right)$$ } d_x, the linear momentum dispersion

$$R_{26} = \left(\theta_n / \delta_0 \right)$$ } d_θ, the angular momentum dispersion

$$R_{51} = \left(\ell / x_0 \right)$$
$$R_{52} = \left(\ell / \theta_0 \right)$$
} terms mixing (x, θ) and(ℓ, δ) co-ordinate pairs in bending magnets

R_{56} – has dimensions of length and represent the effective length of a system for longitudinal co-ordinates.

$$R_{55} = 1$$

$$R_{66} = 1$$

The matrix formalism can be regarded as the first term in Taylor's series and extended to second order via the following equation

$$X_i^{(1)} = \sum_j R_{ij} X_j^{(0)} + \sum_{jk} T_{ijk} X_j^{(0)} X_k^{(0)} \tag{5.4}$$

5.3 THE BEAM MATRIX σ

In accelerator and beam transport systems, the behavior of an individual particle is often of less concern than is the behavior of a bundle of particles (the beam), of which a particle is a member. Multi-dimensional phase ellipse formalism is often used to represent such an aggregate of particles. An extension of the matrix algebra of equation 5.2 provides a convenient means for defining and manipulating this beam. TRANSPORT assumes that the beam may be correctly represented in phase space by an ellipsoid in the six-dimensional co-ordinate system. Transport is a matrix calculation that truncates the problem to either first- or second-order in Taylor expansion about the central trajectory. Particles in a beam are assumed to occupy the volume enclosed by ellipsoid, each representing a possible ray. The sum total of all phase points, the phase space volume, is commonly referred to as "phase space" occupied by the beam. The validity and interpretations of this phase ellipse formalism must be ascertained for each system being designed. However, in general, for charged particle beams in accelerators, the first order phase ellipse formalism of TRANSPORT is a reasonable representation of physical reality. The equation of an n-dimensional ellipsoid may be represented in matrix form as:

$$X(0)^T \sigma(0)^{-1} X(0) = 1 \tag{5.5}$$

Where $X(0)^T$ is the transpose of the co-ordinate vector X(0), and σ(0) is a real, positive definite, symmetric matrix.

The volume of the n dimensional ellipsoid defined by sigma is $\left[\pi^{n/2} / \Gamma\left(n/2 + 1\right)\right] (\det \sigma)^{1/2}$. The area of the projection in one plane is $A = \pi (\det \sigma_1)^{1/2}$, where σ_1 the sub-matrix is corresponding to the given plane. This is the "phase space" occupied by the beam.

As a particle passes through a system of beamline components such as drift spaces and dipole magnets its behavior in the six dimensional spaces, defined above, is described by successive multiplication of the matrices for the individual beamline components with the vector **X**, according to the transformation given by equation 5.2. Combining the transformation with the equation of the initial ellipsoid (5.5), and using the identity matrix, $RR^{-1} = I$ (the unity matrix), it follows that:

$$X(0)^T \left[R^T R^{T^{-1}}\right] \sigma(0)^{-1} \left[R^{-1} R\right] X(0) = 1 \tag{5.6}$$

From which we obtain:

$$\left[RX(0)\right]^T \left[R\sigma(0)R^T\right]^{-1} \left[RX(0)\right] = 1 \tag{5.7}$$

The equation of the ellipsoid representing the "BEAM" at the end of the system is thus:

$$X(1)^T \sigma(1)^{-1} X(1) = 1$$

(5.8)

Where the equation for the sigma matrix at the end is be related to that at the beginning by:

$$\sigma(1) = R\sigma(0)R^T \tag{5.9}$$

In addition to calculating the product matrix, TRANSPORT also computes the sigma "BEAM" matrix at the end of each physical element via equation 5.9. All of the important physical parameters of the BEAM ellipsoid maybe expressed as functions of the matrix elements of the sigma matrix at the location in question. In particular the square roots of the diagonal elements $\left(\sqrt{\sigma ii}\right)$ are the projection of the ellipse upon the coordinate axes and thus represent the maximum extent of the BEAM in the various coordinate directions. The correlation between components (the orientation of the ellipse) is determined by the off-diagonal terms (the σij)'s.

5.4 DESCRIPTION OF THE SIGMA BEAM MATRIX

Consider a 2-dimentional (x, θ) plane projection of the general 6-dimensional ellipsoid.

Let
$$\sigma = \begin{bmatrix} \sigma_{11} & \sigma_{21} \\ \sigma_{21} & \sigma_{22} \end{bmatrix} \tag{5.10}$$

Be a real, positive definite, symmetric matrix; the inverse of the matrix is given by;

$$\sigma^{-1} = \left(\frac{1}{\varepsilon^2}\right) = \begin{bmatrix} \sigma_{22} & -\sigma_{21} \\ -\sigma_{21} & \sigma_{11} \end{bmatrix} \tag{5.11}$$

Where ε^2 is the determinant of the sigma matrix.

The 2-dimensional coordinate vector and its transpose are:

$$X = \begin{bmatrix} x \\ \theta \end{bmatrix} \quad \text{and} \quad X^T = [x \quad \theta] \tag{5.12}$$

The expansion of the matrix equation (5.8) is the equation of the ellipse

$$\sigma_{22} x^2 - 2\sigma_{21} x\,\theta + \sigma_{11}\theta^2 = \varepsilon^2 = \det\sigma \tag{5.13}$$

The (x, θ) plane BEAM ellipse represented by equation 5.13 is shown in the following figure along with the physical meaning of the sigma matrix elements **[BRO77].**

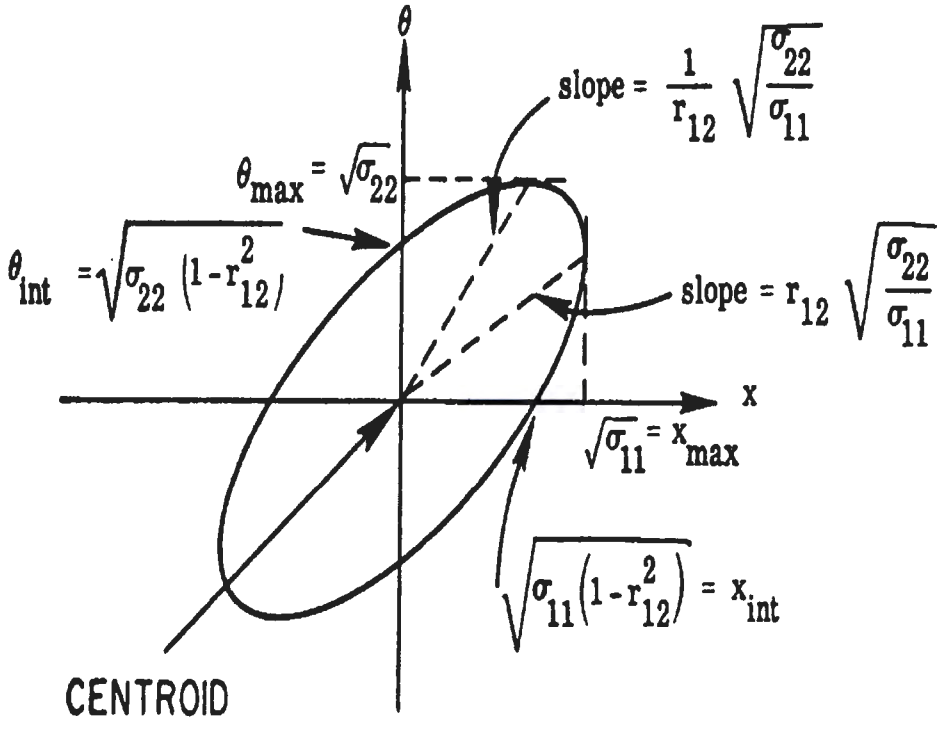

Figure 5.1: A two Dimensional BEAM Phase Ellipse

The area of an ellipse is given by:

$$A = \pi(\det\sigma)^{1/2}$$

$$= \pi x_{max}\theta_{int}$$

$$= \pi x_{int}\theta_{max} \tag{5.14}$$

The correlation between x and θ (the orientation of the ellipse) depends upon the off-diagonal term σ_{21}. This correlation is defined as

$$r_{21} = r_{12} = \frac{\sigma_{21}}{\sqrt{\sigma_{11}\sigma_{22}}} \tag{5.15}$$

So defined r always falls in the range

$$-1 \le r \le 1$$

The correlation, r, measures the tilt of the ellipse and the intersection of the ellipse with the coordinate axes.

5.5 THE PHASE SPACE ELLIPSE BEAM MATRIX USED BY TRANSPORT

For static magnetic systems possessing midplane symmetry, the (x, θ) plane and (y, ϕ) plane trajectories are decoupled in first-order. However, to allow for the possibility of more general systems, the sigma BEAM matrix used in a TRANSPORT calculation has the following general

6-dimensional construction and is printed out in the format shown in table 5.1[**BRO77**].

	x	θ	y	φ	ℓ	δ
x	σ(11)					
θ	σ(21)	σ(22)				
y	σ(31)	σ(32)	σ(33)			
φ	σ(41)	σ(42)	σ(43)	σ(44)		
ℓ	σ(51)	σ(52)	σ(53)	σ(54)	σ(55)	
δ	σ(61)	σ(62)	σ(63)	σ(64)	σ(65)	σ(66)

Table 5.1: The sigma matrix used in TRANSPORT

The matrix is symmetric so that only a triangle of elements is needed. In the printed output the matrix has a different format for ease of interpretation. The matrix σ is used for the beamline design and is printed out in the format shown in table 5.2 **[BRO77, MAI02]**

			x	θ	y	φ	ℓ
x	$\sqrt{\sigma(11)}$	CM					
θ	$\sqrt{\sigma(22)}$	MR	r(21)				
y	$\sqrt{\sigma(33)}$	CM	r(31)	r(32)			
φ	$\sqrt{\sigma(44)}$	MR	r(41)	r(42)	r(43)		
ℓ	$\sqrt{\sigma(55)}$	CM	r(51)	r(52)	r(53)	r(54)	
δ	$\sqrt{\sigma(66)}$	PC	r(61)	r(62)	r(63)	r(64)	r(65)

Table 5.2: The sigma matrix results from TRANSPORT

NWU LIBRARY

where : $r(ij) = \dfrac{\sigma(ij)}{[\sigma(ii)\sigma(jj)]^{1/2}}$

As a result of the fact that the σ matrix is positive definite, the r(ij) satisfy the relation

$$|r(ij)| \leq 1.$$

In brief, the physical meaning of the $\sqrt{\sigma(ii)}$ is as follows:

$\sqrt{\sigma(11)} = x_{max}$ = the maximum (half)-width of the beam envelope in the x (bend)-plane at the point of the print out.

$\sqrt{\sigma(22)} = \theta_{max}$ = the maximum (half)-angular divergence of the beam envelope in the x (bend) plane.

$\sqrt{\sigma(33)} = y_{max}$ = the maximum (half)-height of the beam envelope

$\sqrt{\sigma(44)} = \phi_{max}$ = the maximum half angular divergence of the beam envelope in the y (non-end) plane.

$\sqrt{\sigma(55)} = \ell_{max}$ = one-half the longitudinal extent of the bunch of particles

$\sqrt{\sigma(66)} = \delta$ = the half width ($\frac{1}{2}\Delta p/p$) of the momentum interval being transmitted by the system.

The units appearing next to the $\sqrt{\sigma(ii)}$'s in the TRNSPORT print out sheet are the units chosen for the co-ordinates $x, \theta, y, \varphi, \ell$ and $\delta = \Delta p/p$ respectively.

5.6 GEOMETRIC LIGHT OPTICS VS MAGNETIC OPTICS

Figure 5.2 shows a thin lens with a ray leaving a focal point A at an angle θ_0, impinging on the lens at x_0. As the ray leaves the lens, it is at x_1 and going towards a focal point B at an angle of θ_1.

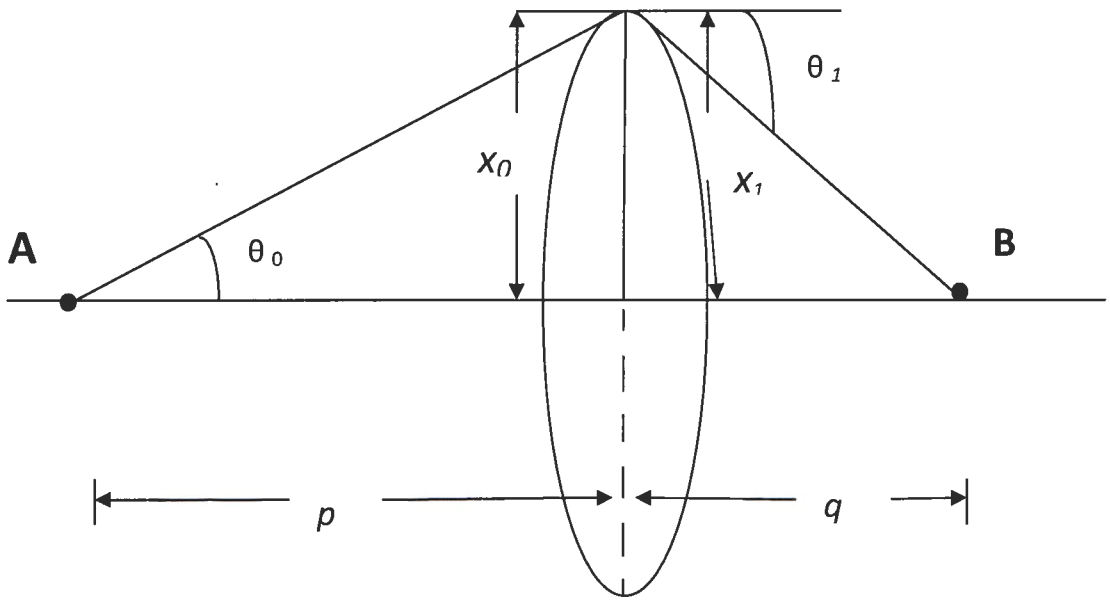

Figure 5.2: Diagram showing a thin lens with a ray leaving a focal point A going towards focal point B

According to the following thin lens equation:

$$1/p + 1/q = 1/f$$

The matrix transformation for the lens action between principal planes is given as :

$$\begin{bmatrix} x_1 \\ \theta_1 \end{bmatrix} = \begin{bmatrix} 1 & 0 \\ -1/f & 1 \end{bmatrix} \begin{bmatrix} x_0 \\ \theta_0 \end{bmatrix}$$

The transformation for a drift distance L is illustrated in figure 5.3.

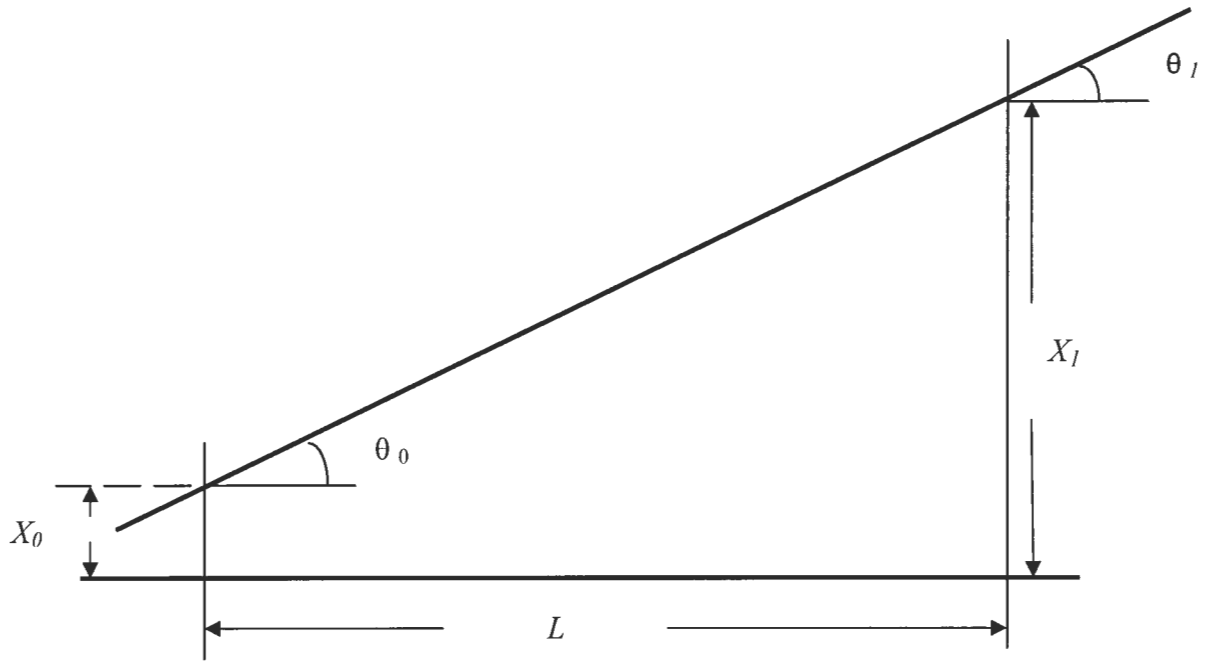

Figure 5.3: A diagram showing the transformation for a drift distance.

$$\begin{bmatrix} x \\ \theta_1 \end{bmatrix} = \begin{bmatrix} 1 & L \\ 0 & 1 \end{bmatrix} \begin{bmatrix} x_0 \\ \theta_0 \end{bmatrix}$$

The determinant of the matrix in both examples is equal to unity. This is a manifestation of Liouville' s theorem of conservation of phase space which state that that the phase-space distribution function is constant along the trajectories of the system - that is that the density of system points in the vicinity of a given system point travelling through phase-space is constant with time.

5.7 INTRODUCTION OF MOMENTUM DISPERSION INTO THE MATRIX FORMALISM

The first order dispersion may be taken into consideration by introducing a 3X3 matrix as follows:

Consider two particles of momentum Po and Po +ΔP passing through the midplane of a static magnetic field, as illustrated in figure 5.4.

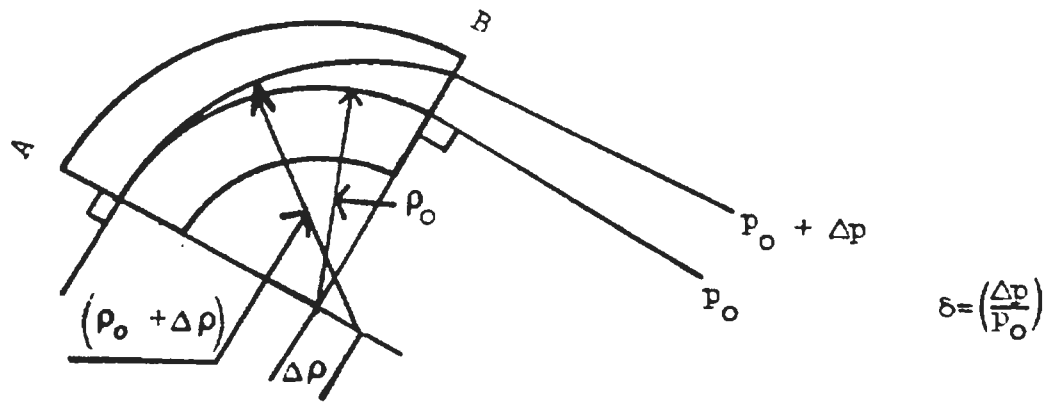

Figure 5.4: Two particles of momentum P_0 and ΔP passing through the midplane of a static magnetic field

Since the scalar momentum of a particle constant is a static magnetic field, the transport equation from A to B may be expressed as

$$\begin{bmatrix} x_1 \\ \theta_1 \\ \delta \end{bmatrix} = \begin{bmatrix} R_{11} & R_{12} & d \\ R_{21} & R_{22} & d' \\ 0 & 0 & 1 \end{bmatrix} \begin{bmatrix} x_0 \\ \theta_0 \\ \delta \end{bmatrix}$$

Where:

$\delta = \Delta P/P0$

d = the spatial momentum dispersion

d' = the derivative of the dispersion (the angular momentum dispersion)

1 = a carrying term to generate a square matrix and denote a constant momentum

The determinant of the matrix [R] is equal to 1 as for the2 X 2 matrix. However, because of the zeros in the bottom row, the fact that $[R] = (R_{11} R_{22} - R_{12} R_{21}) = 1$ only checks the 2 X 2 matrix and not the terms containing d and d'.

Consider now a general system from an object point A to an image point B as shown in figure 5.5.

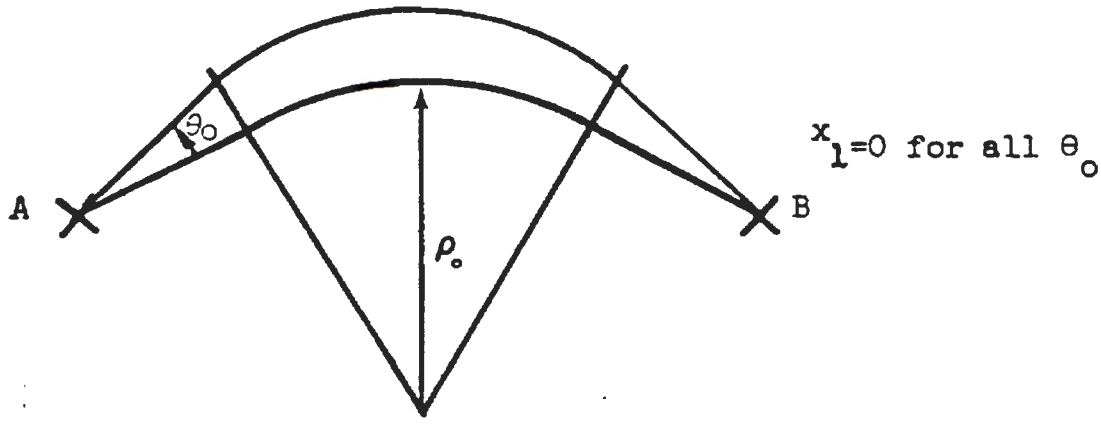

Figure 5.5: A general system from an object point A to an image point B

The above matrix equation is still valid for midplane trajectories. If A is a source point and if $R_{12}=0$ (i.e. the independent of θ_0), then B is an image point for mono-energetic particles.

Under these circumstances:

$R_{11}= M_x$ is the x plane magnification

$R_{22} = 1/M_x$ because det $R=1$

and $R_{21} = -1/f_x$

In fact, $R_{21}= -1/f_x$ for the system between A and B, even if A and B are not foci.

It is now convenient to develop a more general definition of the matrix elements R_{ij} and at the same time introduce the first order matrix transformation for the y plane. Consider, again a general system where the projection of the central trajectory is allowed to bend in the x plane but is a straight line in the y-plane. The x-plane and y-plane matrix transformation may be written as follows:

For the x-plane $x_1=R_x x_0$

Or
$$\begin{bmatrix} x_1 \\ \theta_1 \\ \delta \end{bmatrix} = \begin{bmatrix} c_x(t) & s_x(t) & d_x(t) \\ c_x'(t) & s_x'(t) & d_x'(t) \\ 0 & 0 & 1 \end{bmatrix} \cdot \begin{bmatrix} x_0 \\ \theta_0 \\ \delta \end{bmatrix}$$

Similarly the y-plane, $y_1=R_y y_0$

or

NWU LIBRARY

$$\begin{bmatrix} y_1 \\ \phi_1 \end{bmatrix} = \begin{bmatrix} c_y(t) & s_y(t) \\ c_y'(t) & s_y'(t) \end{bmatrix} \begin{bmatrix} y_0 \\ \phi_0 \end{bmatrix}$$

The c and s functions may be defined in terms of their initial conditions. Let τ be the distance measured along the central trajectory as illustrated by the figure below.

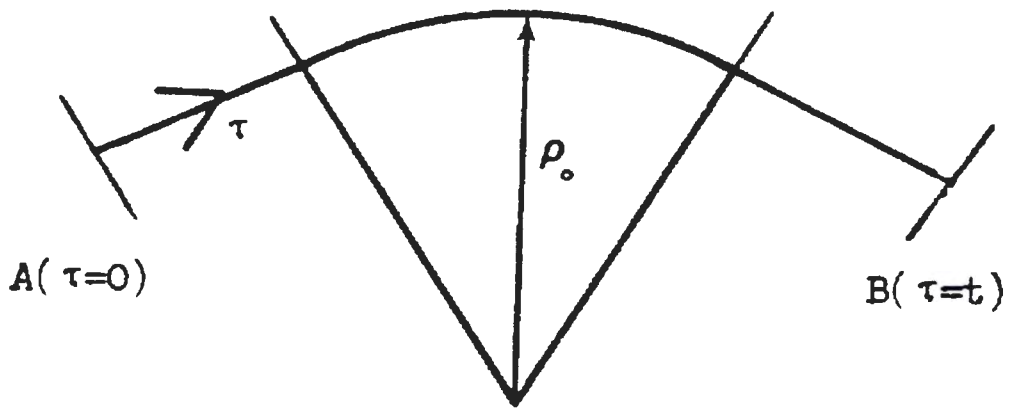

Figure 5.6: Diagram showing the distance measured along the central trajectory

Then:

$$s(0)=0 \qquad s'(0)=1 \quad \text{where} \quad s'(\tau)=\frac{ds(\tau)}{d\tau}$$

$$c(0)=1 \qquad c'(0)=0 \qquad c'(\tau)=\frac{dc(\tau)}{d\tau}=-\frac{1}{f}$$

within an "ideal" magnet, where the bending radius ρ_0 is constant, s and c are sine and cosine or else sinh and cosh functions.

By analogy whenever $s(\tau)=0$, we are at an image of point A. Also, $c(\tau)$ at the position where $s(\tau)=0$ is the magnification of point A at that image.

$$c'(t)=-1/f$$

where f is the focal length of the system between A and B. The dispersion d_x may be derived from the general differential equations of motion of a charged particle in a static magnetic field. The results may be expressed as a function of s_x and c_x as follows:

$$d_x(t)=s_x(t)\int_0^t c_x(\tau)d\alpha - c_x(t)\int_0^t s_x(\tau)d\alpha$$

And

$$d'_x(t)=s'_x(t)\int_0^t c_x(\tau)d\alpha - c'_x(t)\int_0^t s_x(\tau)d\alpha$$

Where

$$d\alpha=\frac{d\tau}{\rho_0(\tau)}$$

is the differential angle of the central trajectory. At an image point $[s(t)=0]$ note that

$$d_x(t)=-c(t)\int_0^t s(\tau)d\alpha$$

CHAPTER 6

CHARGE EXCHANGE CELL DESIGN

6.1 Introduction

It has been evident that the use of hydrogen gas as a charge exchange medium was by no means ideal for production of negative helium ions. The work of Donally **[DON67]** offered a new approach to the problem. He proposed the use of an alkali vapor for charge exchange in order to get higher exchange efficiency. He suggested that this charge exchange reaction is a two step process as presented in chapter 3. He showed that at very low positive energies, about 2 keV, in an exchange medium of cesium vapor, a close to resonant process occurred leading to a very large cross-sections for the formation of He^-. Other alkali metal vapours can also be used. With the selection of charge exchange medium the following factors should be considered:

1. The energy of the ions
2. The ionization potential
3. The vapor must be metallic
4. Electron affinity

Schlachter et al **[SCH68]**, Girnius et al **[GIR76],** Heinemeier et al **[HEI78]**, Ennis et al **[ENN67]**, Middleton and Adams [**MID67]** described experiments with negative Helium ion sources in which cesium, Rubidium, Sodium, Potassium and lithium were used as exchange vapours. The maximum He^- yield of 1.4% is found at about 6keV for cesium, 1.7% at about

7keV for Rubidium, 1.7% at about 7.5keV-12keV for potassium, 1.7% at 12keV for Sodium and above 20 keV for lithium. Although lithium produces maximum He^- at sufficient temperatures, above 20keV, it requires frequent maximum maintenance owing to the condensation of lithium. Lorents et al **[LOR65]** found that the total charge transfer cross section for - Cs collision to be 1.66 $X10^{-14}$ cm^2 at a energy of 2keV. They point out that this very large cross section is probably due to the nearly resonant charge transfer to excited state of He. The maximum yield of He^- ions after passage of a beam through Cs vapor is shown as a function of energy in Figure 6.1. The Cs target thickness necessary for a maximum yield of He^- is 5 $X10^{14}$ atoms/cm^2. The use of very low positive energy is the disadvantage in tandem accelerator applications. Na also have large He^- yield but it requires higher operating temperature to give adequate vapor pressure therefore we find either Cs or Rb easier to handle than the other alkali metals because they melt at relatively low temperatures.

The negative helium ion source described in this dissertation, Rubidium (Rb) vapor is used for charge exchange because of its low electron affinity and lower atomic number which minimizes the multiple scattering of the ion beam. Rb is also using higher positive ion energy than Cs and the resulting negative ions from Rb are also produced at higher energies and this of critical importance in the operation of Tandem where negative ions must be introduced at higher energies in order to avoid beam scattering preferably approaching 100keV. The maximum yield of He^- ions for various values of the energy of the incident ion is shown in figure 6.2. The maximum He^- fraction occurs when the target thickness is 6 $X10^{14}$ atoms/cm^2 **[GIR76].** Adequate vapor pressure of Rb occurs with temperatures of ~260°C at the reservoir and ~135°C on the walls of the exchange region.

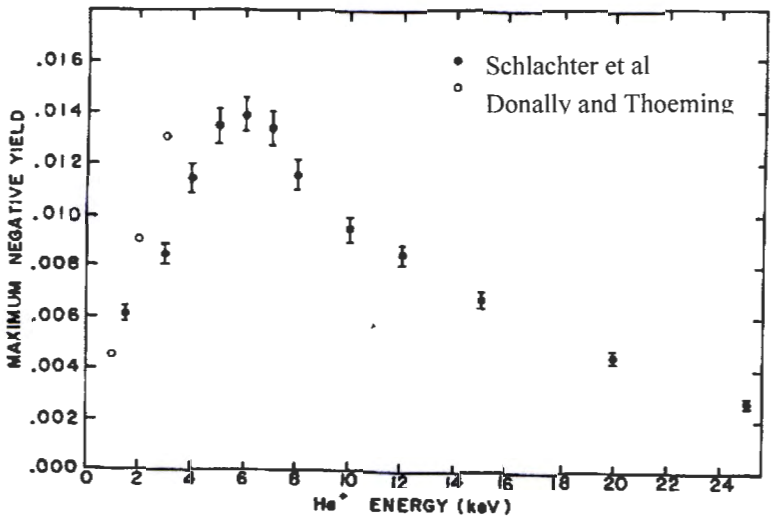

Figure 6.1: The maximum yield of He^- ions after charge exchange in Cs vapor, in the energy range 1.5-25 keV. **[SCH68]**

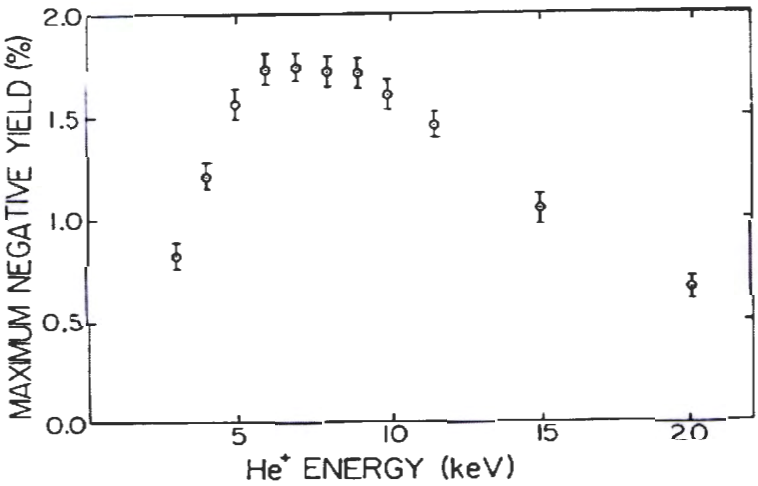

Figure 6.2: The maximum yield of He^- ions after charge exchange in Rb vapor, in the energy range 1.5-20 keV. **[GIR76]**

6.2 THE ION SOURCE

The main requirement is to design an ion source with good qualities. A general feature of source design is to use materials with low sputtering probabilities, high melting points and exclude materials that are likely to introduce impurities in the gas chamber.

6.2.1 DUOPLASMATRON

The positive helium beam is obtained from the duoplasmatron source and focused through the charge exchange canal. The focusing system of the duoplasmatron consists of the expansion cup and the extraction electrode. Details of the duoplasmatron ion source have been published elsewhere **[MOK02]**.

The Duoplasmatron ion source to be used with the present design is the one that already exists at iThemba LABS and has been described by Mokoduwe et al **[MOK02]**. A schematic diagram of the Duoplasmatron source is given in figure 6.3. This Duoplasmatron ion source will generate the ions to be injected into the second stage of the negative source, namely, the charge exchange canal designed in the present work.

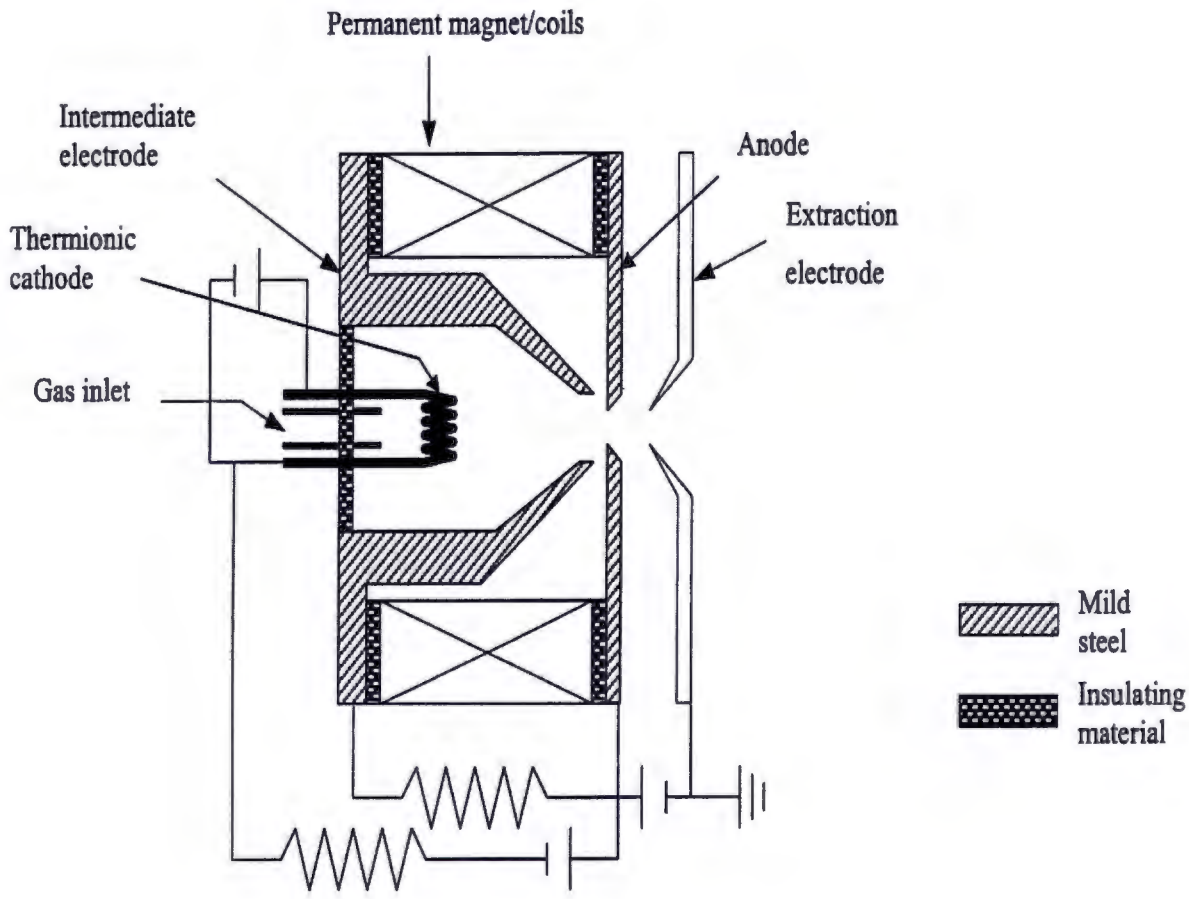

Figure 6.3: Schematic diagram of the discharge chamber of the duoplasmatron ion source **[MOK02].**

6.2.2 THE CHARGE EXCHANGE CANAL

A cross sectional view of a charge exchange cell, designed for production of negative helium ions is displayed in figure 6.4.

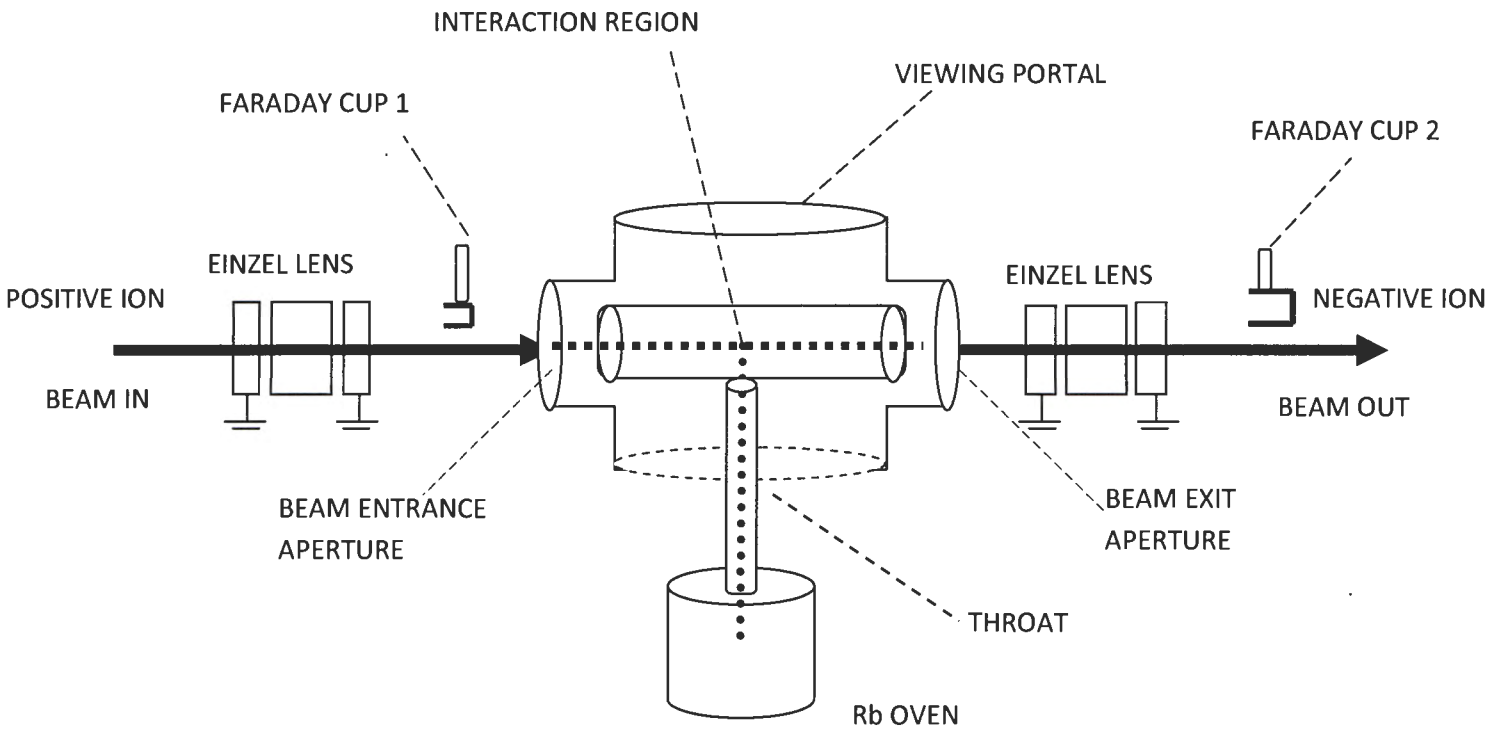

Figure 6.4: A cross-sectional view of a designed charge exchange canal

The cell is equipped with pneumatically actuatable faraday cups, located at the entrance and exit of the cell to aid in characterization of the cell i.e. measuring transmission and charge exchange efficiencies of species of interest in this case positive and negative helium ions. The alkali vapor used for charge exchange is obtained by heating of rubidium (Rb) in the stainless steel container. The cell uses heaters clamped against the body of the stainless steel cell for heating Rb to the temperature that optimizes the vapour density in the path of the beam. A beam of Rb atoms travels up through the connecting tube, the throat, which has a high flow resistance into the charge exchange cell. The rubidium throughput and hence its number density is determined by the reservoir temperature and the conductance of the throat. After several bounces, the Rb atoms sticks to the slope of the inner surface of the exchange cell, gather into liquid droplets and trickle back down into the reservoir. This circulation is further facilitated by a fine stainless steel mesh

covering the wall of the throat that acts as a wick. The angle of the slope in the interaction region is a critical parameter for proper recirculation which depends on the material used. The temperature gradient is maintained by heating the reservoir and cooling the upper part of the throat using water-cooled copper block, fixed to its top.

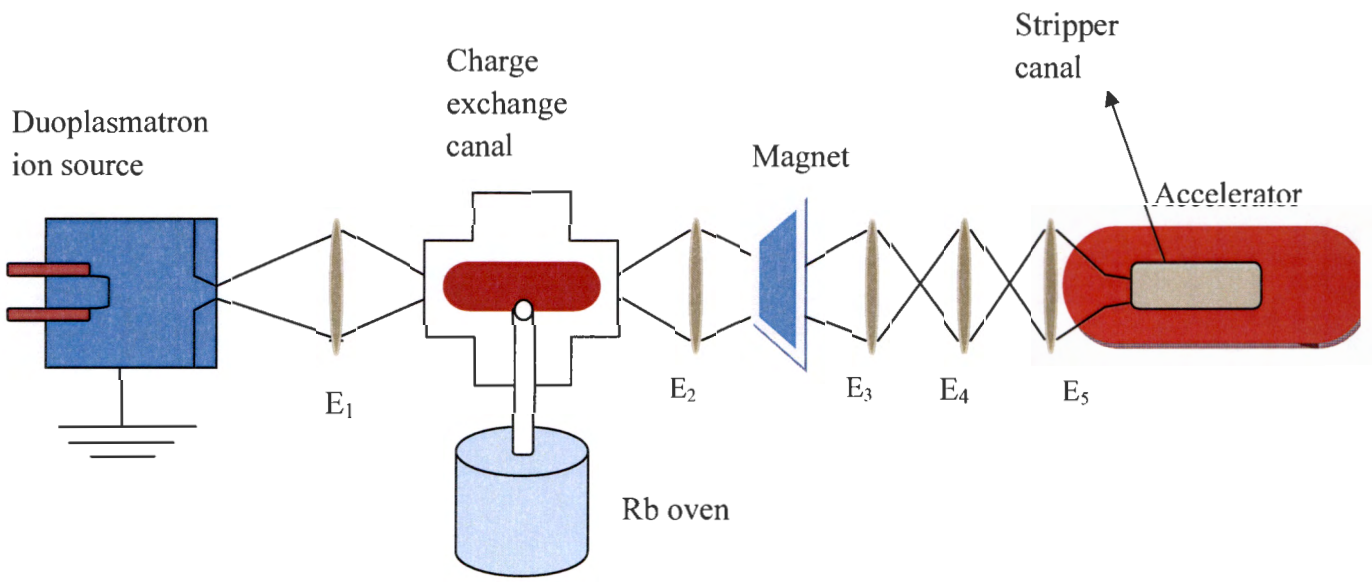

Figure 6.5: A diagram of ion beam apparatus

Our apparatus as illustrated in Figure 6.5 consists of basically 5 parts, the Duoplasmatron positive ion source, set of 5 Einzel lenses E_1, E_2, E_3, E_4 and E_5, a charge exchange canal, magnet and an accelerator. Positive helium ions are produced by the Duoplasmatron ion source in the first stage. Usually the positive ion source is at ground potential and the extraction electrode and donor canal at a common adjustable negative potential V. In the second stage the positive beam from the Duoplasmatron ion source is then focused by an Einzel lens into the charge-exchange region, where the beam passes through a canal filled with rubidium vapor from a heated rubidium reservoir, in which a small fraction of the positive beam will be converted to negative

helium ions. After charge exchange the negative ions are accelerated back to ground potential and emerge with energy of 2 × V (eV).

At the focal point, the beam size is estimated to be about 4.5mm in diameter if the longitudinal size of the charge exchange cell is 60mm, the aperture sizes of the entrance and exit of the cell can be of the order 8-10mm in diameter. Because the beam diverges strongly due to collisions in the cell, a second set of Einzel lens is placed down stream from the exchange canal in order to reshape the negative beam and form a "beam object" waist for injection into a double focusing 30^0 inflection magnet. The pole-gap of the magnet is 20mm. Subsequently the beam is transported over a ~6.5m distance by a set of 2 Einzel lenses and a "snout" lens into the first section of the Tandem Accelerator. This first stage of acceleration stage consists of two acceleration tubes with about 80 acceleration electrostatic sections formed in an electric gradient towards the central terminal separated by 400μ resistors. At the central terminal the beam enters an 80cm long charge exchange canal of 8mm diameter which imposes one of the major constrains of beam transport through the Tandem accelerator.

The physical dimensions of the beamline and beam optics components described above have been introduced with high precision into the Transport code to simulate the beam transport as accurately as possible. In order to account for possible discrepancies with reality a worse case scenario has been used by introducing a rather larger Emittance in the Duoplasmatron ion source. Direct emittance measurements have not been made but rough estimates can be obtained from the size of the sputtered spot on the cathode.

The intensity of the beam produced by charge exchange depends strongly on its energy, the reason for this is, the space charge of the ions which puts upper limit on the current density than

NWU LIBRARY

can be extracted from an ion source at a particular energy. This upper limit is described by Langmuir's space charge law. According to this law the maximum current density j, may be written as:

$$j = c\frac{u^{3/2}}{\sqrt{M}}$$

where:

u is the acceleration voltage,

M the ion mass number and

c depends only on the geometry of the extraction region of the ion source.

6.3 The calculated beam envelope for the designed beamline

The TRANSPORT input and output files used for the designed beam line up to the position of the stripper pipe of the Tandem accelerator are given in appendix A and B respectively.

The fields and the gradients of different magnetic beam line elements were varied in order to obtain transmission through the beam line and beam waists at the desired positions. The beam envelope for the designed beamline is shown below in figure 6.6. The beam envelope is satisfactory and shows consistency

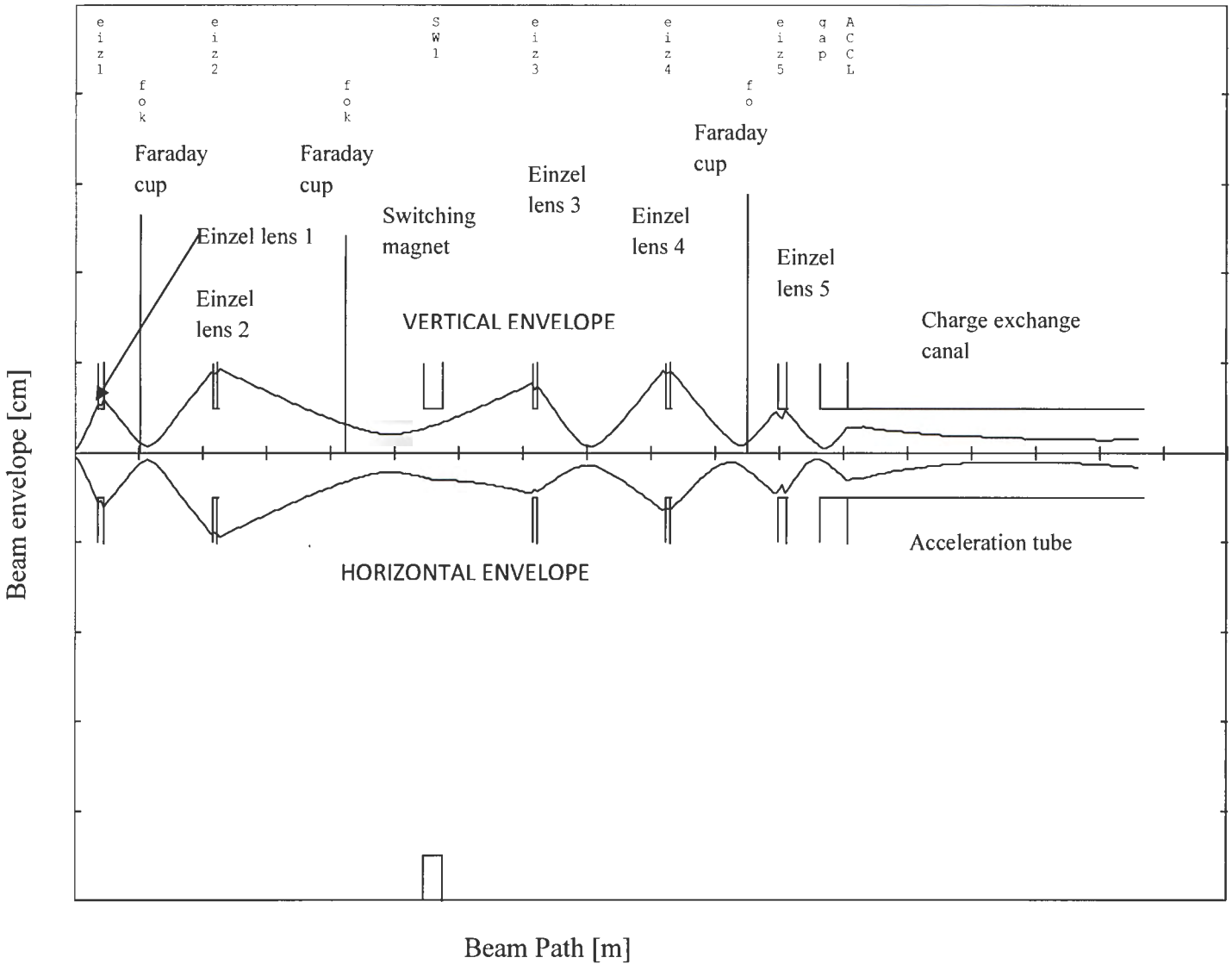

Figure 6.6: TRANSPORT calculations showing the beam envelope from the ion source, through a system consisting of 5 Einzel lenses, a bending magnet and a low energy side of the Tandem up to the position of the stripper pipe.

CHAPTER 7

DISCUSSION AND CONCLUSIONS

The physics of double electron capture through charge exchange atomic collisions have been reviewed in connection with designing a negative helium ion source to be used with the 6 MV EN Tandem electrostatic accelerator of iThemba LABS. The design is based on a two step process of forming /He^- ions, incorporating a duoplasmatron positive ion source and a subsequent charge exchange process. The required optical characteristics of the beam were assessed and guided the design by performing beam optics calculations and simulations using the TRANSPORT code.

The charge exchange process is undoubtedly the most used method of producing negative helium ions and probably the most investigated and best understood process. Basically, duoplasmatron induced positive ions are accelerated through a potential difference and are allowed to traverse a donor medium, usually in the form of vapour or gas. Most of the beam emerges as neutral or positive ions but generally up to 1% emerges as negative ions. The method has the advantage that if the donor canal is at negative potential the positive ion source can be at ground potential and the emerging negative ions on returning to ground potential have been accelerated twice. The additional energy is a distinct advantage for tandem injection as it improves the optical quality of the beam.

A well focused beam source can deliver large current into the Rb vapor cell through a small aperture to produce He^- beam. The ideal beam envelope extracted from a well focused duoplasmatron ion source has been estimated based on Mokoduwe et al **[MOK02]**. It is shown

that a positive helium beam current of the order of 90 micro amps and 85 micro amps can be obtained from that particular positive ion source at extraction voltages of 12kV and 10kV respectively. This also proves that the duoplasmatron ion source is/can be a good source for ions production.

The beam line is designed for optimum transmission of the beam. In this design, the first Einzel lens is used to direct the positive ions from the duoplasmatron to the charge exchange canal. The use of an Einzel lens has the advantage that the charge exchange canal can be of smaller bore which minimizes the vapor flow. In the charge exchange canal the beam defocuses due to multiple atomic collisions over a substantial distance and therefore a second Einzel lens is needed after the charge exchange canal to refocus the beam. A focusing 30^0 bending magnet, for separation of , He^- and unwanted electrons has to be inserted between the source and the existing beamline. The bending magnet is also used to focus the beam in both horizontal and vertical directions. By calculation, using the computer program TRANSPORT, the optimum position and dimensions of the exchange cell have been determined.

The dimensions of the exchange cell must be determined by the emmitance of the beam and vapour loss to the system. Then high He^-/ He^+ yields and intense He^- beams of good stability can be obtained. The beam optics calculations account for a worst case scenario, as the original parameters of the beam-emmitance have been exaggerated on purpose. Still, an almost flat-top transmission is possible by carefully manipulating the Einzel lenses and drift lengths.

For the rather high operating voltages the Duoplasmatron source is working under at iThemba LABS (~20KV) a Li based charge exchange canal would be preferable in terms of high efficiency in production of He^-. However the complications related to Li condensation and

subsequent electrical conductivity and unwanted discharges make Li undesirable as exchange medium.

H.T Richards **[RIC67]** tried Rb as the charge-exchange target in his He^- ion source and he mentioned that Rb is superior to Cs as a target in his source. Currents as large as 14μA of He^- have been obtained from that particular source.

Most laboratories use either Cs or Rb as charge exchange media due to their low electron work function and better charge exchange efficiency as determined by a series of experiments. The maximum He^- yield of 1.4% is found at about 6keV for cesium, 1.7% at about 7keV for Rubidium. Thus, the choice of Rubidium seems to be slightly favorable over Cesium given also the more practical aspects of manipulating Rb rather than Cs. In addition, the Rb's lower atomic number minimizes the multiple scattering of the ion beam at the exchange canal and the resulting negative ions from Rb are also produced at slightly higher energies improving in this manner the beam-optics characteristics of the ion beam.

Beams of adequate intensity and quality will become available when the proposed source is constructed and implemented. Based upon the result of this investigation, it is concluded that this process for negative helium ion production is suitable as a source for tandem accelerators.

APPENDIX A

THE TRANSPORT INPUT FILE USED FOR THE DESIGN OF BEAMLINE IS LISTED BELOW:

```
/New Schonland injection 40 KeV/
0  (indicator card: means the data that follows describes a new problem)
13. 48.0 /ANG/ ;                                  (bending magnet input specification)
15. 1.0 /MM/ 0.1 ;                                (input-output units)
15. 11.0 /MEV/ .001 ;
-15. 6.0 /PM/ 0.1 ;
-16. 14.0 0.0 /SLIT/ ;                            (Print slit aperture)
-16. 31. 0. ;                                     (switch to random search algorithm)
-13. 2 ;
13. 6. ;
                                                  (Transformation matrix will be printed after
                                                   every physical element that follows this code)
1. 1. 30. 1. 30 .627 0.00004932 8.659 /BEAM/ ;    (initial beam parameters)
16. 3.0 1836.69 /MASS/ ;                          (mass of the particles comprising the beam,
                                                      in  units of electron mass)
16. 31. 0. /RAN0/ ;                               (switch to random search algorithm)
16. 22. 100. /NITR/ ;                             (number of steps for random search)
16. 7. 0.4 ;
16. 7. 4.4 ;
3. .035 ;                                         (Drift length)
3. .35 ;
16. 3.0 1836.69 /MASS/ ;                          (mass of the particle comprising the beam  in units
                                                                                  of electron mass)
11. 0.0 0.0135 /eiz1/ ;                           (first Einzel lens)
11. 0.008 1 ;
11. 0.054 1 ;
11. 0.008 0.000 ;
3. .25 ;                                          (Drift length)
3. .277 ;
3. .060 ;
3. 0.001 /fok/ ;                                  (Faraday cup)
3. 0.60 ;
3. .277 ;
3. .25 ;
16. 3.0 1836.69 /MASS/ ;
11. 0.0 0.0072 /eiz2/ ;                           (second Einzel lens)
11. 0.008 1 ;
11. 0.054 1 ;
11. 0.008 0.000 ;
3. 2 /fok/ ;                                      (faraday cup)
```

```
3. 0.50 ;
3. 0.72 ;
2. 0 ;
4. .30368 -30 0.0 /SW1/ ;                (switching magnet at 30^0)
2. 0 ;
3. 1.4 ;
16. 3.0 1836.69 /MASS/ ;
11. 0.0 0.00785 /eiz3/ ;                 (third Einzel lens)
11. 0.008 1 ;
11. 0.054 1 ;
11. 0.008 0.000 ;
3. 1.0 ;
3. 1.0 ;
11. 0.0 0.00858 /eiz4/ ;                 (forth Einzel lens)
11. 0.008 1 ;
11. 0.054 1 ;
11. 0.008 0.000 ;
3. 1 ;
3. .2 /fok/ ;                            (faraday cup)
3. .475 ;
11. 0.0 0.01225 /eiz5/ ;                 (Fifth Einzel lens)
11. 0.008 1 ;
11. 0.127 1 ;
11. 0.008 0.000 ;
3. .025 ;
3. .5 ;
11. 0.0 0.048 /gap/ ;
11. 0.040 1 ;
11. 0.402 1 ;
3. .00001 ;
3. .00001 ; 11. 0.0 5.925 /ACCL/;         (accelerator input parameters)
 11. 0.02538 0.00417 ;
 11. 0.02538 0.00833 ;
 11. 0.02538 0.01184 ;

 11. 0.02538 0.65660 ;
 11. 0.02538 0.66360 ;
 11. 0.02538 0.67061 ;
```

SENTINEL (The data for a given problem is terminated by the word SENTINEL)
/*PLOT*/ (plotting the TRANSPORT run to view the fitted beam envelope)
-1 (Indicator card: means the data that follows describes the changes to be made in the previous step of a given problem)
SENTINEL (The data for a given problem is terminated)

SENTINEL (a second SENTINEL signifies the end of TRANSPORT run)
11. 0.02538 0.00417 ;
11. 0.02538 0.00833 ;
11. 0.02538 0.01184 ;
11. 0.02538 0.01534 ;
11. 0.02538 0.01885 ;
11. 0.02538 0.02235 ;
11. 0.02538 0.02585 ;
11. 0.02538 0.02936 ;

NOTE THAT:

- Each element is given by a sequence of items, mostly numbers that are separated by spaces and terminated by semicolon, which is a requirement to run TRANSPORT. The items, in order, are a type code number, a vary field, the physical parameter and an optional label **[MAI02].**
- The comments given in the appendix are stated to explain the meaning of the different elements in the beam card and are not required when running the TRANSPORT program.

APPENDIX B

THE TRANSPORT OUTPUT FILE

Label	Element	ℓ	x	y	θ	ϕ
BEAM	BEAM	0.000 m	1.00 mm	1.00 mm	0.00 mm/%	0.00mm/%
DRIFT		0.035 m	1.45 mm	1.45 mm	0.00mm/%	0.00mm/%
DRIFT		0.385 m	11.59 mm	11.59 mm	0.00mm/%	0.00mm/%
ACC	Eiz1	0.385 m	11.59 mm	11.59 mm	0.00mm/%	0.00mm/%
ACC		0.393m	10.91 mm	10.91 mm	0.00mm/%	0.00mm/%
ACC		0.447 m	11.24 mm	11.24 mm	0.00mm/%	0.00mm/%
ACC		0.455 m	12.05 mm	12.05 mm	0.00mm/%	0.00mm/%
DRIFT		0.705 m	7.67 mm	7.67 mm	0.00mm/%	0.00mm/%
DRIFT		0.982 m	3.07 mm	3.07 mm	0.00mm/%	0.00mm/%
DRIFT		1.042 m	2.26 mm	2.26 mm	0.00mm/%	0.00mm/%
DRIFT	Fok	1.403 m	2.24 mm	2.24 mm	0.00mm/%	0.00mm/%
DRIFT		1.643 m	9.34 mm	9.34 mm	0.00mm/%	0.00mm/%
DRIFT		1.920 m	14.21 mm	14.21 mm	0.00mm/%	0.00mm/%
DRIFT		2.170 m	18.63 mm	18.63 mm	0.00mm/%	0.00mm/%
ACC	Eiz2	2.170 m	18.63 mm	18.63 mm	0.00mm/%	0.00mm/%
ACC		2.178m	17.96 mm	17.96 mm	0.00mm/%	0.00mm/%
ACC		2.232 m	18.26 mm	18.26 mm	0.00mm/%	0.00mm/%
ACC		2.240 m	17.96 mm	17.96 mm	0.00mm/%	0.00mm/%
DRIFT	fok	4.240 m	19.03 mm	19.03 mm	0.00mm/%	0.00mm/%
DRIFT		4.740 m	4.65 mm	4.65 mm	0.00mm/%	0.00mm/%
DRIFT		5.460 m	5.58 mm	5.58 mm	0.00mm/%	0.00mm/%
ROTAT		5.460 m	5.58 mm	5.58 mm	0.00mm/%	0.00mm/%
BEND	SW1	5.764 m	6.24 mm	7.04 mm	-0.78 mm/%	0.00mm/%
ROTAT		5.764 m	6.24 mm	7.04 mm	-0.78 mm/%	0.00mm/%
DRIFT		7.164 m	9.19 mm	15.65 mm	-7.78 mm/%	0.00mm/%
ACC	Eiz3	7.164 m	9.19 mm	15.65 mm	-7.78 mm/%	0.00mm/%
ACC		7.172 m	8.79 mm	14.97 mm	-7.45 mm/%	0.00mm/%
ACC		7.226 m	8.61 mm	14.69 mm	-7.40 mm/%	0.00mm/%
ACC		7.234 m	8.95 mm	15.28 mm	-7.71 mm/%	0.00mm/%
DRIFT		8.234 m	3.55 mm	2.54 mm	-0.97 mm/%	0.00mm/%
DRIFT		9.234 m	13.15 mm	18.92 mm	5.77 mm/%	0.00mm/%
ACC	Eiz4	9.234 m	13.15 mm	18.92 mm	5.77 mm/%	0.00mm/%
ACC		9.242 m	12.56 mm	18.08 mm	5.53 mm/%	0.00mm/%

ACC		9.296 m	12.49 mm	18.09 mm	5.61 mm/%	0.00mm/%
ACC		9.304 m	13.06 mm	18.93 mm	5.88 mm/%	0.00mm/%
DRIFT		10.304 m	2.30 mm	2.64 mm	2.23 mm/%	0.00mm/%
DRIFT	fok	10.504 m	3.69 mm	2.28 mm	1.50 mm/%	0.00mm/%
DRIFT		10.979 m	9.42 mm	9.62 mm	-0.24 mm/%	0.00mm/%
ACC	Eiz5	10.979 m	9.42 mm	9.62 mm	-0.24 mm/%	0.00mm/%
ACC		10.987 m	8.84 mm	9.06 mm	-0.25 mm/%	0.00mm/%
ACC		11.114 m	8.47 mm	9.10 mm	-0.63 mm/%	0.00mm/%
ACC		11.122 m	8.98 mm	9.68 mm	-0.70 mm/%	0.00mm/%
DRIFT		11.147 m	8.52 mm	9.28 mm	-0.75 mm/%	0.00mm/%
DRIFT		11.647 m	1.86 mm	2.09 mm	-1.78 mm/%	0.00mm/%
ACC	gap	11.647 m	1.86 mm	2.09 mm	-1.78 mm/%	0.00mm/%
ACC		11.687 m	1.78 mm	1.42 mm	-1.42 mm/%	0.00mm/%
ACC		12.089 m	6.24 mm	5.89 mm	-0.30 mm/%	0.00mm/%
DRIFT		12.089 m	6.24 mm	5.89 mm	-0.30 mm/%	0.00mm/%
DRIFT		12.089 m	6.24 mm	5.89 mm	-0.30 mm/%	0.00mm/%
ACC	ACCL	12.089 m	6.24 mm	5.89 mm	-0.30 mm/%	0.00mm/%
ACC		12.114 m	6.13 mm	5.87 mm	-0.21 mm/%	0.00mm/%
ACC		12.139 m	6.03 mm	5.85 mm	-0.13 mm/%	0.00mm/%
ACC		12.241 m	5.85 mm	5.95 mm	0.12 mm/%	0.00mm/%
ACC		12.343 m	5.71 mm	6.04 mm	0.33 mm/%	0.00mm/%
ACC		12.419 m	5.45 mm	5.92mm	0.46 mm/%	0.00mm/%
ACC		12.495 m	5.16 mm	5.73 mm	0.56 mm/%	0.00mm/%
ACC		12.520 m	5.07 mm	5.67 mm	0.62 mm/%	0.00mm/%
ACC		12.596 m	4.81 mm	5.51 mm	0.68 mm/%	0.00mm/%
ACC		12.622 m	4.73 mm	5.46 mm	0.71 mm/%	0.00mm/%
ACC		12.698 m	4.51 mm	5.33 mm	0.79 mm/%	0.00mm/%
ACC		12.723 m	4.44 mm	5.28 mm	0.81mm/%	0.00mm/%
ACC		12.799 m	4.25 mm	5.16 mm	0.88 mm/%	0.00mm/%
ACC		12.825 m	4.18 mm	5.12 mm	0.90 mm/%	0.00mm/%
ACC		12.875 m	4.06 m	5.04 m	0.95 mm/%	0.00mm/%
ACC		12.977 m	3.84 mm	4.90 mm	1.03 mm/%	0.00mm/%
ACC		13.129 m	3.53 mm	4.71 mm	1.15 mm/%	0.00mm/%
ACC		13.358 m	3.14 mm	4.45 mm	1.31 mm/%	0.00mm/%
ACC		13.561 m	2.84 mm	4.25 mm	1.44 mm/%	0.00mm/%
ACC		13.941 m	2.42 mm	3.94 mm	1.66 mm/%	0.00mm/%
ACC		13.967 m	2.40 mm	3.92 mm	1.67 mm/%	0.00mm/%
ACC		14.167 m	2.31 mm	3.89 mm	1.82 mm/%	0.00mm/%
ACC		14.268 m	2.26 mm	3.84 mm	1.88 mm/%	0.00mm/%
ACC		14.471 m	2.17 mm	3.71 mm	1.98 mm/%	0.00mm/%
ACC		14.573 m	2.14 mm	3.66 mm	2.03 mm/%	0.00mm/%
ACC		14.598 m	2.14 mm	3.64 mm	2.04 mm/%	0.00mm/%

ACC		14.700 m	2.13 mm	3.59 mm	2.09 mm/%	0.00mm/%
ACC		14.776 m	2.12 mm	3.55 mm	2.12 mm/%	0.00mm/%
ACC		14.877 m	2.13 mm	3.51 mm	2.17 mm/%	0.00mm/%
ACC		14.903 m	2.13 mm	3.50 mm	2.18 mm/%	0.00mm/%
ACC		14.979 m	2.14 mm	3.46 mm	2.21 mm/%	0.00mm/%
ACC		15.030 m	2.15 mm	3.44 mm	2.23 mm/%	0.00mm/%
ACC		15.207 m	2.20 mm	3.38 mm	2.31 mm/%	0.00mm/%
ACC		15.487 m	2.32 mm	3.29 mm	2.42 mm/%	0.00mm/%
ACC		15.563 m	2.37 mm	3.27 mm	2.45 mm/%	0.00mm/%
ACC		15.791 m	2.50 mm	3.21 mm	2.53 mm/%	0.00mm/%
ACC		15.893 m	2.57 mm	2.57 mm	2.57 mm/%	0.00mm/%
ACC		15.943 m	2.60 mm	3.19 mm	2.59 mm/%	0.00mm/%
ACC		15.969 m	2.62 mm	3.18 mm	2.60 mm/%	0.00mm/%
ACC		15.994 m	2.63 mm	3.18 mm	2.61 mm/%	0.00mm/%
ACC		16.020 m	2.65 mm	3.17 mm	2.62 mm/%	0.00mm/%
ACC		16.045 m	2.67 mm	3.17 mm	2.63 mm/%	0.00mm/%
ACC		16.070 m	2.69 mm	3.16 mm	2.63 mm/%	0.00mm/%
ACC		16.662 m	3.26 mm	3.24 mm	2.95 mm/%	0.00mm/%

NWU LIBRARY

REFERENCES

[ALT93] Alton G. D, Nucl. Inst. And Meth in Phys Research B73 (1993)259

[ALV51] Alvarez L, "Energy doubling in DC Accelerators" Rev Sci Inst 22 (1951) 705

[BAR90] Barrachina R. O, J. Phys B23 (1990) 2321)

[BOH54] Bohr N and Lindhard J. "Electron capture and loss by heavy ions penetrating through matter' Dan.MAT.FYS.MEDD28, no 7(1954)

[BRO77] Brown K.L, F Rothacker, D.C Carey and Ch Iselin "TRANSPORT: A computer program for designing charged particle beam transport systems, SLAC 91 (Rev. 2)1977, pg 129.

[CAR81] David. C. Carey, "High-energy charged particles optics computer programs in Charged Particle optics" (H. Wolli ed.) Nucl. Inst And Meth 187 (1981) pg.97

[Cottereau E] DC accelerators Cottereau E, tandetron, CNRS /Bat 30 avenue de la Terrasse, F- 91198 Gif sur Yvette Cedex,France

[DEM32] A.J. Dempster, Phys Rev 42 (1932) 901

[DON67] B. L Donnally and G. Thoeming, "Helium Negative Ions from Metastable Helium Atoms" Physics Review 159(1967) 87)

[D'YA71] D'Yachkov B. A and Zinenko V. L "High intensity source of He^- ions" Soviet physics- technical physics vol 16 (1971)305).

[ENN67] Ennis et al IEEE. Trans Nuclear SCI-14 (1967) 75

[FAI88] Fainstein et al J. Phys. B: At. Mol. Opt. Phys 21 (1988) 287

[GIL64] Gillespie J 1964 Final-State Interactions (San Fransisco: Holden-Day)

[GIR76] Girnius R. J and Anderson L. W 'Collision of with a Rb vapour target"

Nuclear Instruments and Methods 137 (1976)373-378

[HEI78.1] Heinemeier Jan and Hvelplund Preben, "Production of 15-90 Kev Negative Heavy Ions by Charge Exchange in Mg Vapour" Nuclear instruments and Methods 148(1978) 65-75

[HEI78] Heinemeier Jan and Hvelplund Preben, "Production of 10-80 keV Negative Heavy Ions by Charge Exchange in Na Vapour" Nuclear instruments and methods 148(1978) 425-429.

[HEL05] Hellborg R (Ed) Electrostatic accelerators Fundamentals and applications with a foreword by Kai Siegbahn published 2005.

[HILUP] Ion and electron sources, C.E. Hill unpublished

[HOO80] Hooper, E.B. Jr ; Pincosy, P.A. ; Poulsen, P. ; Burrell, C.F. ; Grisham, L.R. ; Post, D.E. "High current source of He/sup -/ ions" Rev. Sci. Instr. 51 (1980) 1066.

[HOR02] Horsdal-Pedersen, E.; Corke, C.L. Stockli, M.: Experimental observation of the Thomas-peak in high velocity electron capture by proton from He. In Phys. Rev. Sci. Instrum.73(2002), April, No. 4, pp. 1866]

[HOT75] H Hotop and W. C Lineberger " ionization potentials and electron affinities of the elements". J Phys. Chem. Ref. Data 4 (1975) 539

[KEN73] Kenneth H. Purser "Some advances in negative ion technology" University of Rochester and General Ionex Corporation Rochester, New York IEEE 1973).

[LOR65] Lorents D.C and Peterson J.R ., I abstract of papers of the forth International Conference on the Physics of Atomic and Electronic Collisions. Science book

crafters, Inc, Hastings on Hudson, New York , 1965 page 328.

[MAI02] Maine P. M, Conradie J.L and Fourie D.T, "Design and optimization of new beamlines for iThemba LABS. M.Sc. thesis, Centre for Applied Radiation Science and Technology, University of North-West, (2002)

[MID67] Middleton R and Adams T. C. Preliminary notes on the Penn negative helium source, Laboratory Report (University of Pennsylvania, 1967)

[MID71] Middleton R Moylan; Adams T. Charles "Process for production of negative helium ions and other negative ions" university of Pennsylvania Patented Nov. 2, 1971).

[MID83] Middleton R. "A versatile high intensity negative ion source" Nucl. Instr. And. Meth 214 (1983) 139-150

[MOK02] Mokoduwe P.S, Conradie J.L and de Villiers J.G, "Development of a duoplasmatron ion source at iThemba LABS. M.Sc. thesis, Centre for Applied Radiation Science and Technology, University of North-West, (2002)

[RIC67] Richards, H. T. IEEE Trans. Nucl. Sci **NS-14**, no 3 (1967) 78

[SAL72] Salin A J. Phys.B;At Mol. Phys 5 (1972) 979

[SAR89] Sarkadi et al Phys. Rev. Lett.62 (1989)527

[SCH68] Schlachter A et al "Charge-Exchange collisions between Helium ions and Cesium Vapor in the Energy Range 1.5-25keV" Phys Rev 174 (1968)201-211

[SHA27] Shakeshaft, Robin: Spruch, Larry: Mechanism for charge transfer (or for the capture of any light particle) at asymptotically high impact velocities. In

Rev. Mod. Phys. 51(1979), April, No2, pp. 369]

[STO05] "Electron-transfer processes in fast ion-atom collision" Kristian Støchkel, thesis 2005.

[SZA77] Szanto de Toledo A and Sala O "Production of negative helium ions" Instituto de fisica, Universidade de sao Paulo, Sau Paulo SP. Revista Brasileira de fisica, Vol.7, (1977) pg 79

[TAY72] Taylor J.R Scattering theory (New York: Wiley) 1972

[THO27] Thomas L. H. "Calculations of atomic fields" In Proc Soc. London, Ser.A 114(1927) pp 561].

[VOG86] Vogt H. Schuch, R; Justiniano, E;Schulz, M. ; Schwab, W.: Experimental test of higher order electron capture process in collision of fast protons with atomic hydrogen. In Phys Rev. let. 57(1986), November, pp2256-2559]

[WOL95] Wolf Bernhard, HANDBOOK OF ION SOURCES pp. 293, CRC Press, 1995.

[WWW1] http://chem.ch.huji.ac.il/history/graaff.html

[WWW2] http://www.nd.edu/~nsl/html/reseach_SNICS.html

[WWW3] http://hyperphysics.phy-astr.gsu.edu/hbase/quantum/helium.html